INDIAN JOURNAL OF HETEROCYCLIC CHEMISTRY

A Quarterly International Refereed Journal – Published since 1991

Abstracted and Indexed In: SCI Expanded || SCOPUS || CAS || CAB Abstracts || UGC-CARE List Group A || EBSCOhost

Journal DOI 10.59467/IJHC **ISSN 0971-1627**
Journal URL https://connectjournals.com/IJHC **eISSN 2456-4311**

SAMPLE PAPERS

A. Fadil M. Hamed[1], Maitham M. Abdulridha[2] and Bassam A. Hassan[3*] **: Iraq**
B. Xueli Hou[1,2,3,4], Zhewei Zhang[1,2,3,4], Hao Wang[2,3,4], Ze Li[2,3,4], Kai Chen[2,3,4], Yan Luo[2,3,4], Zhenghong Luo[1,2,3,4*] and Zijian Zhao[1,2,3,4*] **: China**
C. Akshita Goel[1,2], Indu Negi[1], Sanchita Aggarwal[1], Ankur Ganesh Pandey[1*] and Purshotam Sharma[1*] **: India**
D. Samy K. El-Desouky **: Kingdom of Saudi Arabia**

Indian Journal of Heterocyclic Chemistry ISSN (Print) : 0971-1627
Vol. 35 - Number 02 (Apr-Jun 2025) 355-362 ISSN (Online) : 2456-4311
https://connectjournals.com/01951.2025.35.355
https://doi.org/10.59467/IJHC.2025.35.355

Design, molecular docking, ADME study, and anticancer evaluation of some new 3-(benzylthio)-5-phenyl-4*H*-1,2,4-triazol-4-amine derivatives

Fadil M. Hamed[1], Maitham M. Abdulridha[2] and Bassam A. Hassan[3*]

[1]Shatrah University, Thi-Qar, 64001, Iraq.
[2]Department of Medical Lab, Shatra Technical College, Southern Technical University, Basra, Iraq.
[3]Department of Pharmaceutical Chemistry, College of Pharmacy, University of Thi-Qar, Thi-Qar, 64001, Iraq.

Indian Journal of Heterocyclic Chemistry ISSN (Print) : 0971-1627
Vol. 35 - Number 02 (Apr-Jun 2025) 189-196 ISSN (Online) : 2456-4311
https://connectjournals.com/01951.2025.35.189
https://doi.org/10.59467/IJHC.2025.35.189

Synthesis and analgesic activity of some new sinomenine derivatives

Xueli Hou[1,2,3,4], Zhewei Zhang[1,2,3,4], Hao Wang[2,3,4], Ze Li[2,3,4], Kai Chen[2,3,4], Yan Luo[2,3,4], Zhenghong Luo[1,2,3,4*] and Zijian Zhao[1,2,3,4*]

[1]Department of Pharmacology, Shaanxi University of Chinese Medicine, Xianyang, China
[2]Department of Pharmaceutical Engineering, College of Chemistry and Materials Engineering, Huaihua University, Huaihua, China
[3]Hunan Provincial Engineering Technology Research Center for Polyvinyl Alcohol Based New Functional Materials, Huaihua, China
[4]Key Laboratory of Research and Utilization of Ethnomedicinal Plant Resources of Hunan Province, Huaihua University, Huaihua, China

Indian Journal of Heterocyclic Chemistry ISSN (Print) : 0971-1627
Vol. 35 - Number 02 (Apr-Jun 2025) 559-568 ISSN (Online) : 2456-4311
https://connectjournals.com/01951.2025.35.559
https://doi.org/10.59467/IJHC.2025.35.559

Toward the development of better therapeutic agents for *Mycobacterium Tuberculosis*: Computational design and evaluation of pyrazinone derivatives as inhibitors of enoyl acyl carrier protein reductase

Akshita Goel[1,2], Indu Negi[1], Sanchita Aggarwal[1], Ankur Ganesh Pandey[1*] and Purshotam Sharma[1*]

[1] Department of Chemistry and Centre of Advanced Studies in Chemistry, Panjab University, Chandigarh, India
[2] Chandigarh Group of Colleges, Jhanjheri, Mohali, Punjab, India

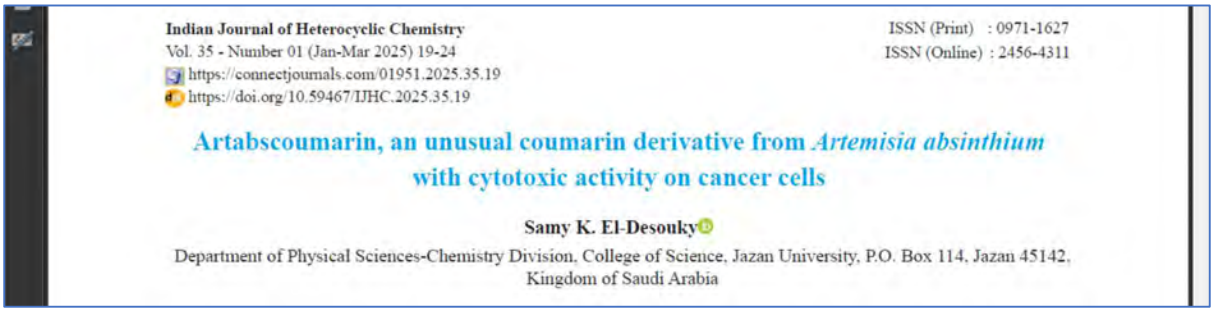

Indian Journal of Heterocyclic Chemistry ISSN (Print) : 0971-1627
Vol. 35 - Number 01 (Jan-Mar 2025) 19-24 ISSN (Online) : 2456-4311
https://connectjournals.com/01951.2025.35.19
https://doi.org/10.59467/IJHC.2025.35.19

Artabscoumarin, an unusual coumarin derivative from *Artemisia absinthium* with cytotoxic activity on cancer cells

Samy K. El-Desouky

Department of Physical Sciences-Chemistry Division, College of Science, Jazan University, P.O. Box 114, Jazan 45142, Kingdom of Saudi Arabia

Indian Journal of Heterocyclic Chemistry
Vol. 35 - Number 02 (Apr-Jun 2025) 355-362
https://connectjournals.com/01951.2025.35.355
https://doi.org/10.59467/IJHC.2025.35.355

ISSN (Print) : 0971-1627
ISSN (Online) : 2456-4311

Design, molecular docking, ADME study, and anticancer evaluation of some new 3-(benzylthio)-5-phenyl-4*H*-1,2,4-triazol-4-amine derivatives

Fadil M. Hamed[1], Maitham M. Abdulridha[2] and Bassam A. Hassan[3]*

[1]Shatrah University, Thi-Qar, 64001, Iraq.
[2]Department of Medical Lab, Shatra Technical College, Southern Technical University, Basra, Iraq.
[3]Department of Pharmaceutical Chemistry, College of Pharmacy, University of Thi-Qar, Thi-Qar, 64001, Iraq.

ABSTRACT Five new 3-(benzylthio)-5-phenyl-4*H*-1,2,4-triazol-4-amine derivatives (**3a-3e**) were synthesized in three steps, starting with benzohydrazide. The last step involved the reaction of 4-amino-5-phenyl-4*H*-1,2,4-triazole-3-thiol **[2]** with benzoyl chloride derivatives in ethanol. The new compounds exhibited anticancer activity docking with C-Met tyrosine kinase receptor, as shown by their docking scores ranging between −3.058 and −4.131 Kcal/mol. Conversely, the binding affinity of crizotinib is −3.223 Kcal/mol regarding antitumor efficacy. Initial anticancer evaluations demonstrated that the compounds display action against HepG2 and Human Neonatal Dermal Fibroblast (HdFn) cell lines. The synthesized compounds had a pronounced cytotoxic effect on the HepG2 cell line, with an IC_{50} of 109.13 µg/mL, while demonstrating a minimal cytotoxic effect on normal human cells (HdFn cell line) with an IC_{50} of 222.17 µg/mL. Absorption, distribution, metabolism, excretion analysis shows that all synthesized derivatives have good theoretical pharmacokinetics and drug-likeness characteristics, making them suitable as oral-derived agents.

KEYWORDS Absorption, distribution, metabolism, excretion, triazole, molecular docking, anticancer, design.

How to cite this article: Hamed, F.M., Abdulridha, M.M. and Hassan, B.A. Design, molecular docking, ADME study, and anticancer evaluation of some new 3-(benzylthio)-5-phenyl-4*H*-1,2,4-triazol-4-amine derivatives, *Indian J. Heterocycl. Chem.*, **2025,** *35*, 355–362. *https://doi.org/10.59467/IJHC.2025.35.355*

INTRODUCTION

Cancer is a category of disorders characterized by the uncontrolled proliferation of cells, infiltration of surrounding tissues, and sometimes metastasis. Strategies to inhibit cell division by targeting the mitotic spindle have long been a fruitful field of study for developing cancer therapeutics.[1] C-Met is a receptor tyrosine kinase present in both normal and cancerous cells. It is a cell surface receptor for the multifunctional cytokine hepatocyte growth factor (HGF), which conveys a specific array of promigratory, anti-apoptotic, and mitogenic signals.[2-6] The pleiotropic effects of the HGF/c-Met axis are essential for tissue homeostasis and development in normal physiological conditions. "A diverse array of human malignancies, including those of the brain, colon, stomach, lungs, breast, and head-and-neck areas, exhibit abnormal HGF/c-Met signaling. Moreover, worse clinical outcomes for cancer patients have been associated with both MET amplification and c-Met overexpression. Amplification of the MET oncogene is seen in EGFR-mutant non-small-cell lung carcinomas after the failure of tyrosine kinase inhibitors."[7-13]

Triazoles are heterocyclic chemical compounds characterized by a five-membered ring structure containing three nitrogen atoms. Two types of triazoles, 1,2,4-triazole and 1,2,3-triazole, as shown in **Figure 1**, have been investigated for their potential as antibacterial agents and inhibitors of enzymes like carbonic anhydrase.[12,14-19]

Recent studies on nitrogen-containing heterocyclic compounds, namely novel 3-(benzylthio)-5-phenyl-4*H*-1,2,4-triazol-4-amine derivatives, have garnered significant attention due to their potential uses, notably in medicine. Numerous pharmaceutical agents, including antimicrobial,

*Corresponding author: Email: bassamalsafee@utq.edu.iq

Published & Hosted by :
Journal Homepage :
www.connectjournals.com/ijhc
www.connectjournals.com

antifungal, antibacterial, antimycobacterial, antiviral, anticancer, antitubercular, antimycotic, antimigraine, anti-inflammatory, analgesic, anticonvulsant, antinociceptive, anti-urease, antioxidant, central nervous system (CNS) stimulant, and antidepressant properties,[20-22] incorporate 1,2,4-triazole rings. 1,2,4-Triazole derivatives have been investigated for their potential medicinal efficacy, including their role as precursors in drug synthesis and prospective anticancer agents. Their potential as a fluorescent probe for imaging biological systems has also been examined.[23-25]

RESULTS AND DISCUSSION

Five new 3-(benzylthio)-5-phenyl-4*H*-1,2,4-triazol-4-amine derivatives (3a-3e) were synthesized in three steps, starting with benzohydrazide, as shown in **Scheme 1**. In Step I, 2-mercapto-5-phenyloxazole (**1**) was prepared from benzohydrazide using the standard method involving the reaction with CS_2 and KOH in ethanol,[25] In Step II, compound was treated with hydrazine hydrate in the presence of KOH in pyridine to give 4-amino-5-phenyl-4*H*-1,2,4-triazole-3-thiol (**2**).[26] Finally, target compounds **3a-e** were obtained by reacting compound **2** with benzyl chloride derivatives. The structures of new compounds were confirmed by spectral and elemental analytical data [**Table 1**].

Molecular docking study

Molecular docking is increasingly vital for drug development. The key objectives are to evaluate ligand-protein affinity and to attain a ligand-receptor complex with an optimum shape and reduced binding free energy. The molecular docking investigation indicates that the newly synthesized chemicals demonstrated an anticancer impact. The anticancer actions of these drugs target the C-Met tyrosine kinase receptor, exhibiting varying scores. Their docking scores vary from −3.058 to −4.131 Kcal/mol, while the binding affinity of crizotinib is −3.211 Kcal/mol. Compound (3b) had the maximum binding affinity of −4.131 Kcal/mol. Upon docking into the C-Met tyrosine kinase receptor, several drugs have anticancer effects with varying binding affinities, as illustrated in **[Table 2].** They establish hydrogen bonds

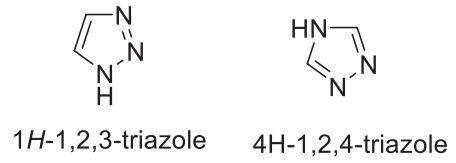

Figure 1: Structure of triazoles

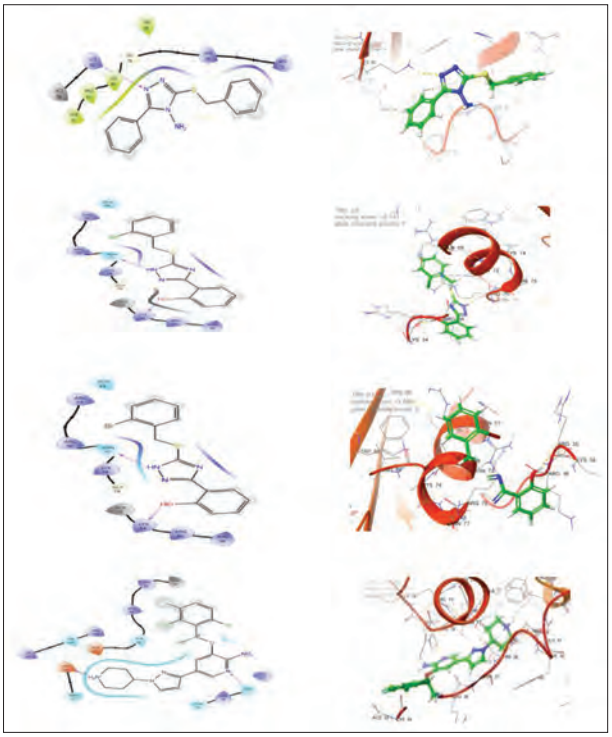

Figure 2: D2 and D3-dimensional representations of molecular interactions between c-met tyrosine inhibitor and (3a, 3b, 3C, and crizotinib drug)

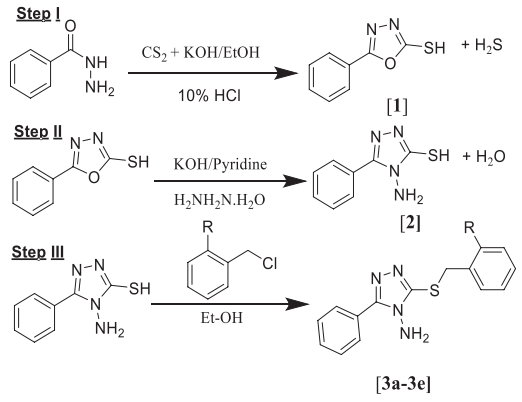

R = 3a=H: 3b= Cl: 3c= Br: 3d= F: 3e=I

Scheme 1: Synthesis of 3-(benzylthio)-5-phenyl-4H-1,2,4-triazol-4-amine derivatives

Table 1: Elemental analyses of compounds 3a-d

Title	Found			Calculated		
	C%	H%	*n*%	C%	H%	*n*%
3a	63.76	5.05	19.70	63.80	5.00	19.84
3b	56.61	4.21	17.54	56.87	4.14	17.68
3c	49.82	3.71	15.69	49.87	3.63	15.51
3d	59.98	4.36	18.80	59.98	4.36	18.65
3e	44.13	3.21	13.94	44.13	3.21	13.72

Table 2: Results of molecular interaction between c-met tyrosine inhibitor, compounds (3a-3e), and reference crizotinib drug

Title	Docking score on E.R.- (Kcal/mol)	H-bond	Others bonds
3a	**−3.058**	LYS 60	------
3b	**−4.131**	ASN 77, LYS 34	------
3c	**−3.898**	ASN 77, LYS 34	------
Crizotinib drug	−3.211	ASP 123, ASN 77	Salt bridge with ASP 123

(H-bonds) with amino acid residues at the protein receptor's active site and supplementary brief contacts that augment the interaction. Compound (3a) binds through three H-bonds with LYS 60. Compound (3b) interacts with the receptor by two hydrogen bridges with ASN 77 and LYS 34. Compound (3c) establishes two hydrogen connections between ASN 77 and LYS 34. In addition, crizotinib establishes two hydrogen connections with ASN 77 and LYS 34 and forms a salt bridge with ASP 123, as described in **Figure 2** and **Table 2.**[14,27-30]

Anticancer activity (cytotoxic effect of the synthesized compounds on hepG2 and human neonatal dermal fibroblast (HdFn) cell line

As illustrated in **Table 3,** Hep G2 (or HepG2) is a human hepatic carcinoma cell line. HepG2 [HEPG2] is a cell line displaying an epithelial-like appearance derived from hepatocellular carcinoma in a 15-year-old Caucasian male from Argentina with liver cancer. The Wistar Institute provided the cell line and an appropriate transfection host-cellular lines. HDFn is a human cell line. The HDFn cell line, derived from the neonatal foreskin, is utilized in research concerning pathogen response, skin aging, wound healing, gene delivery, and skin disorders such as scleroderma. The produced compounds' cytotoxicity **(3a–3e)** was assessed in comparison to the MTT test, which uses HepG2 and HdFn cell lines, based on the color shift of 3-(4,5-dimethyl-2-thiazolyl)bromide-2,5-diphenyl-2*H*-tetrazolium from yellow to purple when viable cells are exposed to apoptosis. Following the maintenance of the plates utilized for a single day at physiological temperature and in the presence of CO_2, specific concentrations of synthesized compounds (3a-3e) were administered at 25, 50, 100, 200, and 400 µg/mL concentrations. The IC_{50} results, representing the half-maximal inhibitory concentration, indicated that the synthesized compound (**3b)** exhibits anticancer activity, although at varying levels influenced by the functional substitution groups of the compounds.

In addition, the number of doses employed suggests that anticancer activity is directly proportional to the increasing concentrations of the administered drugs. It demonstrates negligible efficacy at low concentrations. Various parameters, including lipophilicity and van der Waals volume, influence it. The outcomes of the anticancer activities data of (**3b**) are presented in **Table 3**.[31-36] The synthesized compound (**3b**) showed an Highly cytotoxic effect on the hepG2 Cell lin (µg/mL 109.13), whereas it showed low cytotoxic effect on the human normal Cell (HdFn Cell line) (µg/mL 222.17).

Table 3: Cytotoxic effects of 3b at different concentrations on hepG2 and HdFn

3b	HdFn		hepG2	
Conc.	mean	S.D.	mean	SD
400	74.03533	3.80334	53.1435	2.662674
200	75.556	2.59158	60.4375	2.91264
100	80.142	3.681820	71.2533	1.745590
50	93.11134	2.746873	89.28867	1.691248
25	90.753	2.561253	92.71487	0.867998

SD: Standard deviation

Absorption, distribution, metabolism, excretion (ADME) study results

Essential physicochemical characteristics, lipophilicity, water solubility, pharmacokinetics, drug-likeness, and medicinal chemistry may be determined using the Swiss ADME Web application to speed drug-likeness and radar

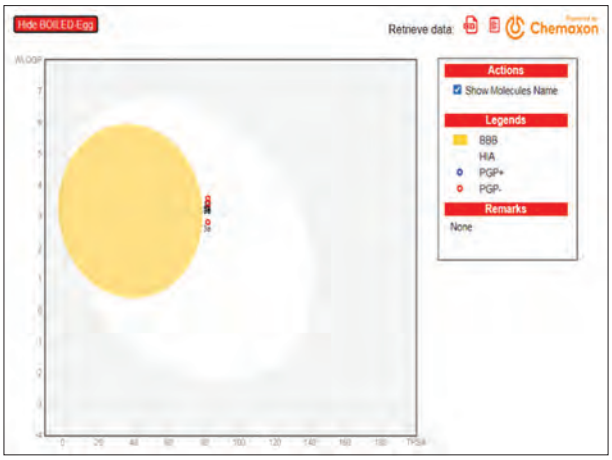

Figure 3: BOILED egg polt of synthesized compound (3a-3e) from the Swiss ADME web tool

Table 4: Physicochemical properties of synthesized compounds (3a-3c)

Compound	3a	3b	3c
Formula	$C_{15}H_{14}N_4S$	$C_{15}H_{13}ClN_4S$	$C_{15}H_{13}BrN_4S$
Molecular weight	282.36 g/mol	316.81 g/mol	361.26 g/mol
Num. heavy atoms	20	21	21
Num. from. heavy atoms	17	17	17
Fraction Csp3	0.07	0.07	0.07
Num. rotatable bonds	4	4	4
Num. H-bond acceptors	2	2	2
Num. H-bond donors	1	1	1
Molar refractivity	81.81	86.82	89.51
Log K_p (skin permeation)	−5.76 cm/s	−5.53 cm/s	−5.76 cm/s

Table 5: Drug likeness, bioactivity, and synthetic accessibility score (3a and 3b)

Drug likeness	3a	3b
Lipinski	Yes, 0 violations	Yes, 0 violations
Ghose	Yes, 0 violations	Yes, 0 violations
Veber	Yes, 0 violations	Yes, 0 violations
Egan	Yes, 0 violations	Yes, 0 violations
Muegge	Yes, 0 violations	Yes, 0 violations
Bioavailability score	0.55	0.55

evaluation. The six physicochemical qualities considered are lipophilicity, size, polarity, solubility, unsaturation, and flexibility. There is a pink region in which the radar plot of the molecule must fall entirely for it to be termed drug-like, and it is projected that the chemical is bioavailable when taken orally, as illustrated in **Table 4.**

Lipinski's parameter rule is a set of guidelines used in drug discovery to evaluate the likelihood of a compound's success as a drug. The rule states that a compound is more likely to be orally active and have good pharmacokinetic properties if it meets the following criteria: Molecular weight ≤500. MLog P ≤ 4.15, N or O ≤ 10, NH or OH ≤ 5.

ADME results of compounds **3a** and **3b** showed, according to Lipinski's rule, that there are no violations with drug likeness, and according to Lipinski, it is close to drug-likeness, as illustrated in **Table 5.**

ADME results of compounds **3a-3e** showed the solubility parameter in water that the log S (ESOL) range is soluble for all compounds **3a-3e**; solubility refers to the ability of

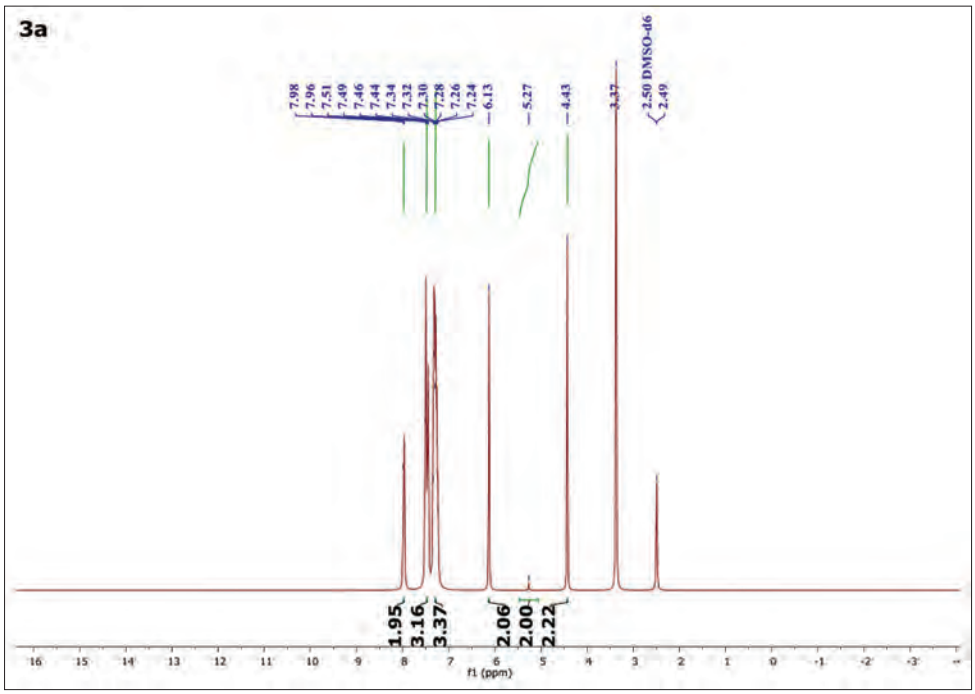

Figure 4: ^{1}H-NMR Spectrum of Compound 3-(benzylthio)-5-phenyl-4H-1,2,4-triazol-4-amine (3a)

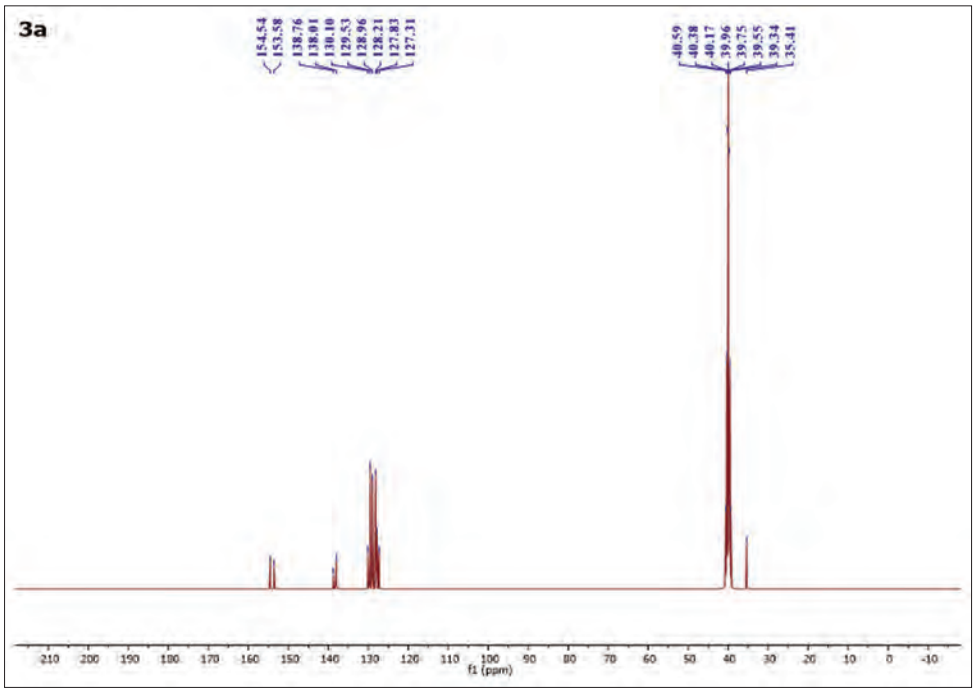

Figure 5: ^{13}C-NMR Spectrum of Compound 3-(benzylthio)-5-phenyl-4H-1,2,4-triazol-4-amine (3a)

a molecule to dissolve in a particular solvent. This property is important because many biological processes occur in aqueous environments, and solubility affects how well a molecule can be transported.

An important parameter in the ADME study is solubility in water measured by log S; the solubility of compounds is classified according to the following log *S* scale:

"insoluble < − 10 < poorly < − 6 < moderately < − 4 < soluble < − 2 < very < 0 < highly."

According to the ADME results, the solubility parameter in water showed a log S (ESOL) range of synthesized compounds **3a-3e** between −5.12 and −3.96, which are soluble depending on the log S scale.

Topological surface area (**TPSA**): The results of the Swiss ADME tool showed that the TPSA of the most synthesized compounds **(3a-3e)** has a TPSA < 121 Å^2 (82.03 Å^2). Indicates favorable characteristics for membrane permeability and oral bioavailability, making the compound potentially more suitable for development as an orally administered drug. Systems. The compounds do not face membrane permeability and oral bioavailability challenges. GIT absorption occurs:

These compounds **3a-3e** showed high GIT absorption; this may be important for drugs intended to target compound oral bioavailability.

And showed not crossing the blood–brain barrier (BBB), which suggests that the compound is not likely to cross the BBB and not reach the CNS. This may not be suitable for drugs intended to target the brain or central nervous system, as BBB permeability is a crucial factor in determining the ability of a compound to exert pharmacological effects within the brain, as illustrated in **Figure 3** and **Table 6**, BOILED egg polt of compounds (**3a-3e**) from the Swiss ADME web tool.

EXPERIMENTAL SECTION

All chemicals and reagents were procured from reputable suppliers, including Sigma-Aldrich and Merck (India), and utilized without purification. Freshly distilled solvents were used throughout the study. The purity of the material was determined by thin-layer chromatography (TLC) on pre-coated silica gel 60 F254 plates. The mobile phase for TLC comprised a combination of chloroform and methanol in an 8:2 volume ratio. Infrared (I.R.) spectra were obtained utilizing a PerkinElmer Tonsor 27 Bruker spectrometer from Germany, outfitted with KBr optics at Thi-Qar University/College of Science. The ^{13}C and ^{1}H NMR spectra were acquired in dimethyl-d6 sulfoxide (DMSO-*d6*) with a Bruker BioSpin GmbH 400 MHz spectrometer at Albasrah University/College of Education. The mass spectrometer recorded the mass spectrum (M.S.) utilizing a Network Mass Selective Detector (5973) at an energy of 70 eV at the University of Tehran, Iran. The instrumentation and stringent evaluation techniques combined emphasize the dependability and precision of the experimental approaches in this research.

5-Phenyl-1,3,4-oxadiazole-2-thiol[1]

A solution was prepared by mixing benzohydrazide (0.68 g, 0.005 moles) and KOH (0.28 g, 0.005 moles) in 70 mL of 100% ethanol, to which CS_2 (0.4 g, 0.005 moles) was gradually introduced at 0°C. The mixture was refluxed for 14–15 h. The evolution of black H_2S gas (on lead acetate paper) indicated the progress of the reaction. The reaction mixture was acidified with 10% hydrochloric acid, and the resultant solid was filtered, washed with water, dried, and recrystallized from ethanol.[37-39] Yield: 91%, Color: Pink, Melting point: 220–222°C.[40]

4-Amino-5-phenyl-4*H*-1,2,4-triazole-3-thiol[2]

A solution was prepared by mixing compound **1 (**1 g, 0.005 mole) and KOH (0.28 g, 0.005 mole) in 100 mL of pyridine, followed by the addition of hydrazine hydrate (0.25 g, 0.005 mole) to the mixture. The solution was refluxed for 12 h. The reaction was monitored by TLC using an eluent of hexane (6) and ethyl acetate (4). The solution was concentrated and subsequently acidified with 10% HCl. The precipitated material was filtered, washed with water, and recrystallized from ethanol.[34,41] Yield: 90%, White needles, melting point: 189–191°C.[42]

Synthesis of 3-(benzylthio)-5-phenyl-4*H*-1,2,4-triazol-4-amine derivatives [3a-3e]

A solution was made by combining compounds **2 (**2g, 0.01 mole) and benzyl chloride derivatives (0.5g, 0.01 mole) in 50 ml of 100% ethanol, which was subsequently heated under reflux for 3 h until HCl evolved. The TLC monitored the reaction using an eluent of hexane (6) and ethyl acetate (4). The reaction solution was concentrated and cooled to room temperature. The mixture was filtered, rinsed with water, and then recrystallized from methanol.[42-47]

3a: Yield 72%, color white, mp 221–223°C,

3b: Yield 70%, color white, mp 223–225°C,

Table 6: Predicted pharmacokinetics and water solubility of compounds 3a-3e

Druglikeness	3a	3b	3c	3d	3e
Log Po/w (WLOGP)	2.81	3.46	3.57	3.37	3.41
TPSA	82.03 Å²	82.03 Å²	82.03 Å²	82.03 Å²	82.03 Å²
GI absorption	High	High	High	High	High
BBB permeant	No	No	No	No	No
Log S (ESOL)	−3.96	−4.54	−4.85	−4.10	−5.12
Water solubility class	Soluble	Soluble	Soluble	Soluble	Soluble

TPSA: Topological surface area

3c: Yield 73%, color white, mp 221–223°C,

3d: Yield 75%, color white, mp 225–227°C

3e: Yield 71%, color white, mp 228–230°C

3a, FT-IR (KBr) cm^{-1}: 3405 (N-H); 3035Ar (C-H); (C-H); 2990, (C-H); 1630, 1612 (C=N);

691(C-N); ^{1}H NMR (400 MHz, DMSO-d6) δ (ppm) as illustrated in **Figure 4**, 4.43 (s,2H, CH_2, δ 5.27 (s,2H, NH_2), 6.13 (m, 2H, ArH), 7.24–7.34 (d, *J* = 8.01 Hz, 3H, ArH), 7.44–7.50 (d, *J* = 7.5 Hz, 3H, ArH), 7. 96–7.98 (d, *J* = 7.2 Hz, 2H, ArH).

^{13}C NMR (101MHz) δ 154.54 (C=N-S), (C=N-Ar) 153.58, (carbon of aromatic ring) 138.76, 138.01, 130.10, 129.53, 128.96, 128.21, 127.83, 127.31, 40.59, 40.38, 40.17, 39.96, 39.75, 39.55, 39.34, (CH_2) 35.41 [as illustrated in **Figure 5**].

3b, FT-IR (KBr) cm^{-1}: 3410 (N-H); 3031Ar(C-H); 2995, (C-H); 1629, 1605(C=N); 652(C-N);

^{1}H NMR (400 MHz, DMSO-d6) δ (ppm)

4.51 (s,2H, CH_2), δ 5.31 (s,2H, NH_2), 6.21 (m, 2H, ArH), 7.32–7.41 (d, *J* = 8.79 Hz, 3H, ArH), 7.69–7.74 (d, *J* = 7.4 Hz, 3H, ArH), 7. 32–7.54 (d, *J* = 7.2 Hz, 2H, ArH).

^{13}C NMR (101MHz) δ 155.52 (C=N-S), (C=N-Ar) 156.32, (carbon of aromatic ring) 139.76, 139.01, 133.10, 128.53, 127.99, 126.20, 125.84, 127.31, 40.59, 40.38, 40.17, 39.96, 39.75, 39.55, 39.34, (CH_2) 35.45.

3c, FT-IR (KBr) cm^{-1}: 3470 (N-H); 3012 Ar (C-H); (C-H); 2945, (C-H); 1621, 1607 (C=N); 690(C-N);

^{1}H NMR (400 MHz, DMSO-d6) δ (ppm)

4.33 (s,2H, CH_2), δ 5.17 (s,2H, NH_2), 6.06 (m, 2H, ArH), 7.41–7.44 (d, *J* = 8.32 Hz, 3H, ArH), 7.55–7.79 (d, *J* = 8.0 Hz, 3H, ArH), 8.46–8.23 (d, *J* = 7.2 Hz, 2H, ArH).

^{13}C NMR (101MHz) δ 164.61 (C=N-S), (C=N-Ar) 166.59, (carbon of aromatic ring) 138.44, 138.21, 135.16, 126.22, 125.21, 124.01, 123.73, 120.32, 40.59, 40.38, 40.17, 39.96, 39.75, 39.55, 39.34, (CH_2) 35.41.

3d, FT-IR (KBr) cm^{-1}: 3402 (N-H); 3070 Ar(C-H); (C-H); 2965, (C-H); 1643, 1621 (C=N); 695(C-N);

^{1}H NMR (400 MHz, DMSO-d6) δ (ppm)

3.93 (s,2H, CH_2), δ 4.92 (s,2H, NH_2), 7.21 (m, 2H, ArH), 7.65–7.72 (d, *J* = 8.23 Hz, 3H, ArH), 7.84–7.96 (d, *J* = 8.15 Hz, 3H, ArH), 8.34–8.41 (d, *J* = 8.65 Hz, 2H, ArH).

^{13}C NMR (101MHz) δ 162.61 (C=N-S), (C=N-Ar) 161.59, (carbon of aromatic ring) 136.41, 135.23, 132.17, 129.24, 128.21, 127.01, 122.73, 121.32, 40.59, 40.38, 40.17, 39.96, 39.75, 39.55, 39.34, (CH_2) 35.40.

3e, FT-IR (KBr) cm^{-1}: 3417 (N-H); 3027Ar(C-H); 2986, (C-H); 1608, 1603 (C=N); 647(C-N);

^{1}H NMR (400 MHz, DMSO-d6) δ (ppm)

4.32 (s,2H, CH_2), δ 5.32 (s,2H, NH_2), 6.65 (m, 2H, ArH), 7.54–7.67 (d, *J* = 8.43 Hz, 3H, ArH), 7.79–7.85 (d, *J* = 8.5 4Hz, 3H, ArH), 8. 30–8.52 (d, *J* = 8.6 Hz, 2H, ArH).

^{13}C NMR (101MHz) δ 164.52 (C=N-S), (C=N-Ar) 162.86, (carbon of aromatic ring) 138.76, 138.01, 136.75, 127.89, 127.78, 126.56, 124.45, 123.23, 40.59, 40.38, 40.17, 39.96, 39.75, 39.55, 39.34, (CH_2) 35.21.

CONCLUSION

This study successfully synthesized new 3-(benzylthio)-5-phenyl-4H-1,2,4-triazol-4-amine derivatives. The newly synthesized compounds exhibited an anticancer effect when docked inside the C-Met tyrosine kinase receptor, as shown by their docking scores ranging from −3.058 and −4.131 Kcal/mol. In contrast, crizotinib binding affinity is −3.223 Kcal/mol for anticancer efficiency. The crystal structure of the C-Met receptor has exhibited activity agents against hepG2 and HdFn cell lines. The synthesized compounds had a cytotoxic effect on the HepG2 cell line, with an IC_{50} of 109.13 µg/mL, while demonstrating a cytotoxic minimal impact on normal human cells (HdFn cell line) with an IC_{50} of 222.17 µg/mL. ADME analysis shows that all synthesized derivatives have good theoretical pharmacokinetics and drug-likeness characteristics, making them suitable as oral-derived agents.

ACKNOWLEDGMENT

This study was supported by the College of Pharmacy, University of Thi-Qar, and the Ministry of Higher Education and Scientific Research, Iraq.

REFERENCES

[1] Mekky, A.H., Hamed, F.M. and Hassan, B.A. Design, synthesis, antibacterial activity, anticancer activity, and molecular docking study of some apocynin derivatives, *Indian J. Heterocycl. Chem.*, **2025**, *35*, 49–55. doi: 10.59467/IJHC.2025.35.49

[2] Abdulridha, M.M. and Mohammed, M.N. Design, synthesis, molecular docking, anticancer and antibacterial activities of some new 4,4'-((((phenylmethylene) bis(4,1-phenylene))bis(oxy)) bis(methylene))bis(1-butyl-1*H*-1,2,3-triazoles, *Indian J. Heterocycl. Chem.*, **2025**, *35*, 77–84. doi: 0.59467/IJHC.2025.35.77

[3] Hassan, B.A. and Mekky, A.H. Synthesis, molecular docking, and anticancer study of some new [1,2,4] triazolo[4,3-b][1,2,4,5]tetrazines, *Indian J. Heterocycl. Chem.*, **2024**, *34*, 391–398. doi: 10.59467/IJHC.2024.34.391

[4] Hasan, B.A. and Abdulridha, M.M. Preparation and characterization of some transition metal complexes of new [butanal (5-Ethyl-1, 3, 4-oxadia-Zol-2-Yl) hydrazone], *Swedish J. Sci. Res.*, **2014**, *1*, 23–36.

[5] Daoud, K.M., Mohamed, S.R. and Al-Niami, N.M. Synthesis of some substituted 1,3,4-oxadiazoles, 1,3,4-thiadiazoles, and 1,2,4-triazoles from 2-(2,3-dimethylphenyl amino) benzoic acid, *J. Educ. Sci.*, **2009**, *22*, 1–10.

[6] Aday, H.A. Synthesis and characterization of the triazole derived from thiosemicarbazide, 4-amino-5- phenyl-4h-1, 2, 4-triazole-3-thiol and their copper (ii) and nickel (ii) complexes, *Eng. Technol. J.*, **2013**, *31*, 216–221.

[7] Dalal, M.J. and Mekky, A.H. Synthesis, characterization and antioxidant evaluation of some tetrazole derivatives, *Indones. J. Chem.*, **2022**, *22*, 1596–1604.

[8] Flifel, I.A., Ajeel, A.K. and AL-Jabery, A.N. Synthesis, characterization and antibacterial study 0f New 2-Ethyl- 5-{[(3-phenyl-5-sulfanyl-4h-1, 2, 4-triazol-4-yl) imino]methyl} benzene-1, 4-diol and their transition metal complexes, *Univ. Thi-Qar J*., **2017**, *12*, 1–20.

[9] Soleiman-Beigi, M. and Mohammadi, F. A novel copper-catalyzed, one-pot synthesis of symmetric organic disulfides from alkyl and aryl halides: Potassium 5-methyl-1,3,4-oxadiazole-2-thiolate as a novel sulfur transfer reagent, *Tetrahedron Lett*., **2012**, *53*, 7028–7030.

[10] Abdulridha, M.M., Hassan, B.A. and Hamed, F.M. Synthesis and antibacterial evaluation of 1,3, 4-thiadiazole containing 1, 3, 4-oxadiazole bearing Schiff bases, *Int. J. Pharm. Res*., **2018**, *10*, 12.

[11] Hassan, B.A., Abdulridha, M.M. and Hamed, F.M. Design and antibacterial activity of 3, 6-diphenyl-1, 5, 6, 7, 8, 8 hexahedron [1, 2, 4]triazolo [4, 3-b][1, 2, 4, 5] tetrazine as fused heterocyclic compounds, *Biochem. Cell. Arch*., **2020**, *20*, 1499–1502.

[12] Hassan, B.A., Baqer, F.M. and Abdulridha, M.M. Design, synthesis and characterization of benzoxazepine thiourea new derivatives, *Int. J. Drug Deliv. Technol*., **2021**, *11*, 874–876.

[13] Hassan, B.A., Nasera, H.N. and Abdulridha, M.M. Synthesis and antimicrobial Evaluation of fused heterocyclic compound [1, 2, 4] triazolo [4, 3-B][1, 2, 4, 5] tetrazine, *Int. J. Res. Pharm. Sci*., **2019**, *10*, 1254–1258.

[14] Hamed, F.M., Hassan, B.A. and Abdulridha, M.M. The antitumor activity of sulfonamides derivatives, *Int. J. Pharm. Res*., **2020**, *12*, 2512–2519.

[15] Witczak, Z.J. and Bielski, R. *New Developments and Strategies. Click Chemistry in Glycoscience*, John Wiley and Sons, United States, **2013**.

[16] Hussain, M.Y., Hassan, B.A. and Hanan, Z.K. Synthesis and characterization of new schiff bass (3Z,3Z)-3,3' -((oxy bis (4,1- phenylene)) bis(azanylylidene)) bis(indolin-2-one), *Turk. J. Comput. Math. Educ*., **2021**, *12*, 3341–3351.

[17] Bassam, A. and Hasan, A. Preparation and characterization of some transition metal complexes of new 4-[(5-ethyl-1, 3, 4-oxadiazol-2-yl) sulfanyl] aniline, *Swedish J. Sci. Res*., **2014**, *1*, 11–23.

[18] Xu, F., Yang, Z.Z., Jiang, J.R., Pan, W.G., Wu, J.Y., Zhu, Y., Wang, J., Shou, Q.Y. and Wu, H.G. Synthesis, antitumor evaluation and molecular docking studies of [1,2,4] triazolo [4, 3-b] [1,2,4,5] tetrazine derivatives, *Bioorg. Med. Chem. Lett*., **2016**, *26*, 3042–3047.

[19] The eel, E. and Mekky, A.H. Synthesis, absorption, distribution, metabolism, excretion, toxicology (ADMET) and molecular docking studies of some pyridin-2 (1h)-one derived from a apocynin in Thi- Qar governorate, *Univ. Thi-Qar J. Sci*., **2023**, *10*, 73–80.

[20] Mahmood, A.A. and Bahnam, S.P. Docking, synthesis and β-lactamase inhibitory activity evaluation for new amide compounds, *Kimya Problemleri*, **2024**, *22*, 139–149.

[21] Abdul-Rida, N.A. and Talib, K.M. New chalcone derivatives as anticancer and Antioxidant agents: Synthesis, molecular docking study, and biological evaluation, *Kimya Problemleri*, 2024, *22*, 177–186.

[22] Flifel, I.A. Synthesis, characterization and anticancer study of new3-[(2z)-2 (2-hydroxybenzylidene) hydrazinyl]-5-(2-hydroxyphenyl)-1,3,4-oxadiazol-3- ium and its transition metal complexes, *Univ. Thi-Qar. J. Sci*., **2023**, *10*, 98–102.

[23] Kamel, M.M. and Abdo, N.Y.M. Synthesis of novel 1,2,4-triazoles, triazolothiadiazines, and triazolothiadiazoles as potential anticancer agents, *Eur. J. Med. Chem*., **2014**, *86*, 75–80.

[24] Nagavelli, V.R., Nukala, S.K., Narsimha, S., Battula, K.S., Tangeda, S.J. and Reddy, Y.N. Synthesis, characterization and biological evaluation of 7-substituted-4-((1-aryl-1h-1, 2, 3-triazol-4-yl) methyl)- 2h-benzo [b][1, 4] oxazin-3 (4*H*)-ones as anticancer agents, *Med. Chem. Res*., **2016**, *25*, 1781–1793.

[25] Hassan, B.A. and Hamed, F.M. Synthesis and pharmaceutical activity of triazole Schiff bases with theoretical characterization, *Kimya Problemleri*, **2024**, *22*, 332–341. doi: 10.32737/2221-8688-2024-3-332-341

[26] El-Reedy, A.A.M. and Soliman, N.K. Synthesis, biological activity, and molecular modeling study of novel 1,2,4-triazolo [4,3-B][1,2,4,5] tetrazines and 1,2,4-triazolo [4,3-b][1,2,4] triazines, *Sci. Rep*., **2020**, *10*, 6137.

[27] Hameed, A.A. and Hassan, F. Synthesis, characterization and Antioxidant activity of some 4-amino-5- phenyl-4*H*-1, 2, 4-triazole-3-thiol derivatives, *Int. J. Appl. Sci. Technol*., **2014**, *4*, 202–211.

[28] Abass, A.A., Muhsin, S.N., Hasan S.A. and Hassan, B.A. Efficacy study of captopril on some liver function tests in hypertensive patients, *Rev. Latinoam. Hipertens*., **2023**, *18*, 142–146.

[29] Abdulridha, M.M, Abdulhussein, H.S., Alyaseen, F.F. and Hassan, B.A. Phytochemical and antibacterial activity of, the *Pegnum harmala* seeds and its alkaloids, *Plant Arch*., **2019**, *19*, 1439–1444.

[30] Shalaal, S.H., Halail, A.T., Hamed, F.M. and Hassan, B.A. Maceration techniques extraction of Thymus vulgaris and laurel (*Laurus nobilis*) leaves with antibacterial study, *Plant Arch*., **2019**, *19*, 4041–4044.

[31] Mohammed, H.M. Synthesis and biological Evaluation of newly sunthesized triazolotriazines and triazolotraizines derivatives, *J. Univ. Anbar Pure Sci*., **2017**, *11*, 25–33.

[32] Musa, M. The prevalence and the significance of the pulmonary bacterial super-infections among hospitalized COVID-19 patients: A scoping review. *Univ. Thi-Qar J. Sci*., **2023**, *10*, 66–72.

[33] Mekky, A.H., Hamed, F.M. and Hassan, B.A. Synthesis, characterization, molecular docking studies, and pharmaceutical Evaluation of some novel [1,2,4] Triazolo[3,4-b][1,3,4] thiadiazole. *J. Kimia Valensi*, 2024, 10, 304–314. doi: 10.15408/jkv.v10i2.40043

[34] Hassan, B.A. and Mekky, A.H. Synthesis, characterization and antibacterial activity of[1,2,4]triazolo[4,3-b] [1,2,4,5]tetrazine derivatives, *Chem. Probl*, **2025**, *25*, 78–94. doi: 10.32737/2221-8688-2025-1-78-94

[35] Pricopie, A.I., Focșan, M., Ionuț, I., Marc, G., Vlase, L., Găină, L.I., Vodnar, D.C., Elemer, S., Barta, G., Pîrnău, A. and Oniga, O. Novel 2, 4-disubstituted-1, 3-thiazole derivatives: Synthesis, anti-*Candida* activity evaluation and interaction with bovine serum albumine, *Molecules*, **2020**, *25*, 1079.

[36] Jabar, D. and Aljaza, D. Conventional and molecular identification of *Candida* spp. and antifungals susceptibility test in pregnant women, *Univ. Thi-Qar J. Sci*., **2022**, *9*, 13–20.

[37] Mammadbayli, E.H. and Babayeva, V.H. Investigation of fungicidal properties of hexyl bromide complex of n'-(2, 2-bicyclo [2.2. 1] hept-5-en-2-yl-4, 5-dihydro- 1-*H*-imidazolin-1-ylethyl) ethane-1, 2-diamine as antimicrobial additive to lubricant-coolant fluids, *Kimya Problemleri*, **2024**, *22*, 168–176.

[38] Suleymanova, A.B., Aliyeva, K.T. and Nasirova, A.E. Chemical composition of extracts and essential oils obtained from common juniper (*Juniperus communis* L.) in Azerbaijan, *Kimya Problemleri*, **2024**, *22*, 211–220.

[39] Akchurina, T., Israfilova, Z., Sadeghian, N., Taslimi, P., Farzaliyev, V., Sujayev, A. and Efendiyeva, K. Synthesis and study of some novel β-arylamino-2-oxy-5-methylpropiophenones as polyethylene stabilizers, *Kimya Problemleri*, **2024**, *22*, 187–196.

[40] Dawood, N.M.Z., Saeed, Z.F. and Saeed, B.B. Synthesis of acetylenic amino derivatives of 2-(2-((2, 6-dichlorophenyl) amino) phenyl) acetic acid, *Kimya Problemleri*, **2024**, *22*, 369–381.

[41] Kerru, N., Gummidi, L., Maddila, S., Gangu, K.K. and Jonnalagadda, S.B. A review on recent advances in nitrogen-containing molecules and their biological applications, *Molecules*, **2020**, *25*, 1909.

[42] Alyaseen, F.F., Hassan, B.A., Abdulhussein, H.S. and Alsafee, B. University of Thi-Qar Extraction, isolation and chemical identification of piperine alkaloid from black pepper seeds and its antibacterial activity, *Plant Arch*., **2018**, *18*, 2171–2176.

[43] Damdoom, W.K., Oday H. Synthesis, characterization of formazan derivatives from isoniazid and study their antioxidant activity and molecular docking. *Russ. J. Bioorg Chem*., **2024**, *50*, 86–94.

[44] Amaral, L.M.P.F, Carvalho, T.M.T. and Da Silva, M.D.M.C.R. Thermochemistry of amino-1, 2, 4-triazole derivatives. *J. Thermal Anal Calorim.*, **2024**, *32*, 1–9.

[45] Shi, H., Li, M., Zhou, Z., Lu, A. and Wang, Z. Synthesis and biological evaluation of novel 1,2,4-triazole derivatives containing amino acid fragments. *Molecules*, **2025**, *30*, 1692.

[46] Abdulghani, S.M., Al-Rawi, M.S. and Tomma, J.H. Synthesis of new 1,2,4-triazole derivatives with expected biological activities, *Chem. Methodol.*, **2022**, *6*, 59-66, doi: 10.22034/chemm.2022.1.6

[47] Hasan, A.Y., Kadh, M.S., Saleh, N.M. and Abou- Amra, E.S. Synthesis of novel [1, 2, 4] triazolo [3, 4-b] [1, 3, 4] thiadiazole-6 (5*H*)-thione, 5, 8-dihydro-[1, 2, 4] triazolo [4, 3-b][1, 2, 4, 5] tetrazine and 5, 10-dihydro-[1, 2, 4] triazolo [4, 3-b][1, 2, 4] benzotriazine derivatives and study their biological activity, *Int. J. Adv. Res*., **2020**, *4*, 335–347.

Received: 18 Apr 2025; Accepted: 25 Apr 2025

Indian Journal of Heterocyclic Chemistry
Vol. 35 - Number 02 (Apr-Jun 2025) 189-196
https://connectjournals.com/01951.2025.35.189
https://doi.org/10.59467/IJHC.2025.35.189

ISSN (Print) : 0971-1627
ISSN (Online) : 2456-4311

Synthesis and analgesic activity of some new sinomenine derivatives

Xueli Hou[1,2,3,4], Zhewei Zhang[1,2,3,4], Hao Wang[2,3,4], Ze Li[2,3,4], Kai Chen[2,3,4], Yan Luo[2,3,4], Zhenghong Luo[1,2,3,4]* and Zijian Zhao[1,2,3,4]*

[1]Department of Pharmacology, Shaanxi University of Chinese Medicine, Xianyang, China
[2]Department of Pharmaceutical Engineering, College of Chemistry and Materials Engineering, Huaihua University, Huaihua, China
[3]Hunan Provincial Engineering Technology Research Center for Polyvinyl Alcohol Based New Functional Materials, Huaihua, China
[4]Key Laboratory of Research and Utilization of Ethnomedicinal Plant Resources of Hunan Province, Huaihua University, Huaihua, China

ABSTRACT In this study, a series of new Sinomenine derivatives **4a**-**4i** were designed and synthesized. The binding energy of the derivatives to the target protein GBP5 was calculated using the molecular docking software MOE, and the possibility of the compounds becoming drugs was predicted using artificial intelligence (AI). Nine sinomenine derivatives were synthesized by modifying the C1 and C4 positions of sinomenine **A** ring. Molecular docking results showed that all the nine derivatives had stable binding to GBP5 protein. AI predicted that the derivative CLogP, oral bioavailability, plasma protein binding rate, blood–brain barrier permeability probability, and blood–brain ratio increased compared with sinomenine. The analgesic activity of the compounds was preliminarily determined by hot plate and acetic acid writhing experiments. The results of the hot plate method showed that the synthesized compounds had some analgesic effects, and the analgesic effects of **4b** and **4f** were better. The results of acetic acid writhing test showed that all the synthesized compounds had some analgesic effects. The analgesic effects of **4a, 4b, 4d, 4e,** and **4g** were better than that of sinomenine, and the other derivatives were equivalent to sinomenine. The results were consistent with the AI prediction results.

KEYWORDS Sinomenine derivatives, Analgesic activity, Molecular docking, Artificial intelligence

How to cite this article: Hou, X., Zhang, Z., Wang, H., Li, Z., Chen, K., Luo, Y., Luo, Z., and Zhao, Z. Synthesis and analgesic activity of some new sinomenine derivatives, *Indian J. Heterocycl. Chem.*, **2025**, *35*, 189–196. *https://doi.org/10.59467/IJHC.2025.35.189*

INTRODUCTION

Rheumatic (Rh) and rheumatoid arthritis (RA) are diseases characterized by pathological changes of joints. According to relevant statistics, the incidence of RA in the population is about 2.5%,[1] and the incidence of Rh in the natural population is about 14.1%.[1] The incidence of specific populations (textile, chemical, underground workers in mining areas, etc.) is as high as 23.1%.[2] Therefore, Rh and RA are diseases that seriously threaten human health.

Sinomenine is an isoquinoline alkaloid isolated from the rhizome of *Sinomenium acutum* Rehd.et Wils.[3] Sinomenine is a clinically effective drug for the treatment of Rh and RA.[4] Sinomenine has a wide range of pharmacological effects, including anti-inflammatory,[5] analgesia,[6] immune regulation,[7] and neuroprotection.[8] At present, the research of sinomenine has achieved many gratifying results. However, Sinomenine has some disadvantages, as follows: short half-life,[9] low bioavailability,[10] gastrointestinal reactions,[11] allergic reactions,[12] and other side effects, as well as poor transdermal absorption.[13] Preparation research can solve its shortcomings to some extent, but it cannot fundamentally change the above deficiencies. To solve the problem fundamentally, it also depends on the in-depth study and breakthrough of pharmaceutical chemistry.

*Corresponding author: Email: 772348112@qq.com; 2447151770@qq.com

Published & Hosted by :
Journal Homepage :
www.connectjournals.com/ijhc
www.connectjournals.com

It is an important and effective way to develop new drugs by modifying and modifying the structure of natural traditional chinese medicine active ingredients or lead compounds, screening and finding new active ingredients or lead compounds, so as to improve drug efficacy, improve their functions, and reduce their toxic and side effects. Nowadays, many scholars have modified the structure of sinomenine and found many compounds with good curative effect.[14]

A literature review of sinomenine found that GBP5 is a potential target for sinomenine in inflammatory cells. Sinomenine directly binds to GBP5, inhibits its activity, regulates P2X7R, and inhibits downstream NLRP3-induced inflammatory pathways. Molecular docking showed that sinomenine could bind to the active pocket of GBP5 with a strong binding energy of −7.72 kcal/mol.[15] In this study, we combined the previous research results of the project group to introduce halogen atoms and benzoic acid at the C1 and C4 positions of the sinomenine A ring.[16] Through molecular docking, AI prediction, acetic acid writhing, and hot plate experiments with GBP5, they were preliminarily screened for activity. The sinomenine derivatives are shown in **Scheme 1**.

RESULTS AND DISCUSSION

Molecular docking

The results of molecular docking are shown in **Table 1**. Using MOE software, the binding energy of GBP5 protein to sinomenine was −6.6513 kcal/mol. Nine derivatives were docked with GBP5, and their binding energy was less than that of sinomenine.

Druggability analysis

ADMET prediction refers to the prediction of a series of key characteristics of drugs *in vivo*. The predicted CLogP of sinomenine was 2.02, the oral bioavailability was 20%, the plasma protein binding rate was 53%, the blood–brain barrier permeability probability was 0.98, the blood–brain ratio was −0.23, the human clearance value was 1.14 (excretion), and DILI was 0.17 (liver injury). Compared with sinomenine, the ClogP of each derivative increased, and the fat solubility increased. Oral bioavailability increased by 12–25%, **4g, 4f, 4a, and 4d** higher, of which **4g** reached 45%, the lowest **4d** reached 38%. The plasma protein binding rate increased by 30–36% as compared to sinomenine, of which **4b, 4d, 4f, 4g, and 4i** was 89%, and the lowest **4c** was 83%. The probability of blood–brain barrier permeability decreased by 0.13–0.47, but the overall was above 0.50, and the blood–brain ratio increased by 0.42–0.9. And combined with the two, **4g, 4d, 4e,** and **4a** are the most advantageous among the nine derivatives. The probability of CYP induction was 0.01–0.04 lower than that of sinomenine, and the probability of each derivative being metabolized in the liver was lower than that of sinomenine, of which **4i** was 0.12, at the lowest value. The human clearance values of **4a, 4b,** and **4c** increased by 0.06, 0.05, and 0.09 as compared to sinomenine, and the probability of human excretion of drugs increased, which was easier to be excreted. Compared with sinomenine, **4d-4i** decreased by 0–0.17 and was less likely to

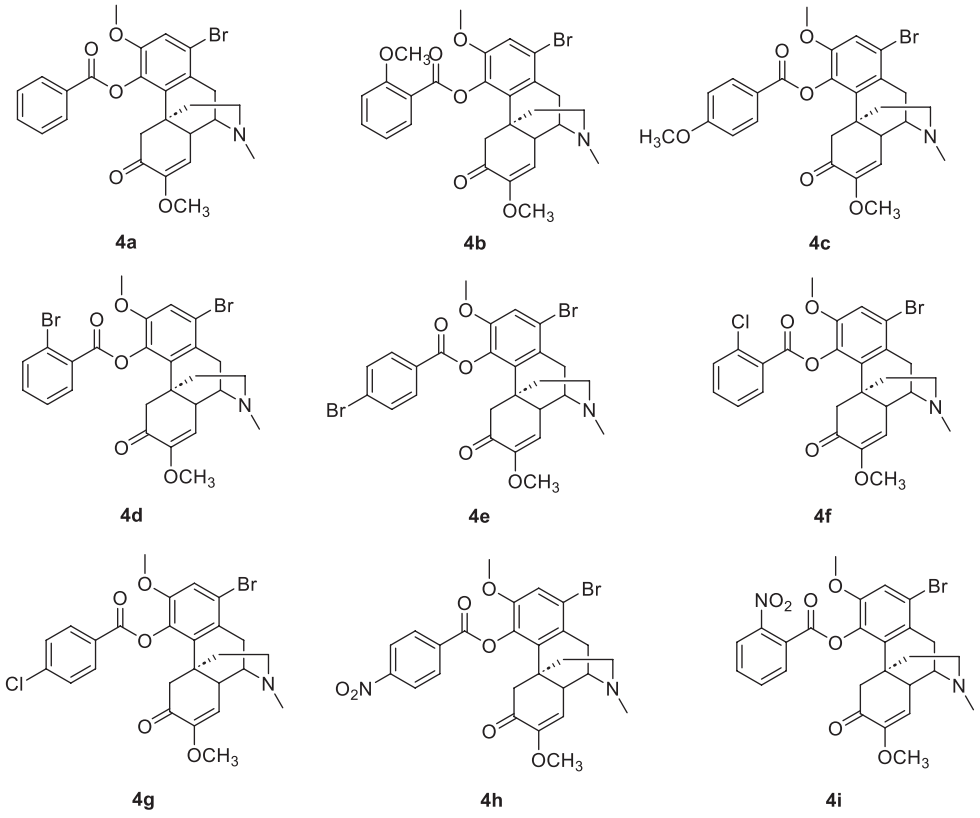

Scheme 1: Sinomenine derivatives 4a-i

Table 1: Molecular docking score of sinomenine and sinomenine derivatives

Model	Binding energy (kcal/mol)
Sinomenine	−6.6513
4a	−7.2701
4b	−7.5382
4c	−7.8191
4d	−7.4405
4e	−7.5110
4f	−7.3724
4g	−7.6019
4h	−8.2157
4i	−7.8446

be excreted. The DILI (probability of liver injury) value was 0.11–0.26 higher than that of sinomenine, indicating that the derivatives had certain hepatotoxicity than sinomenine. The results of druggability analysis are shown in **Table 2**.

Synthesis

The target sinomenine derivatives **4a-i** were synthesized according to the reactions sequence, as shown in **Scheme 2**. First, **1** was treated with 5% NaOH was added to obtain **2**. Then, bromination of 2 with NBS in dichloromethane to gave **3**. In the last step, **3** was converted to the target compounds **4a-i** by the reaction of benzoic acid derivatives using two catalysts, 4-dimethylaminopyridine (DMAP) and 1-(3-Dimethylaminopropyl)-3-ethylcarbodiimide (EDC).

Hot plate method

The hot plate results are shown in **Table 3**. The middle dose of **4a, 4b, 4d, and 4f** high and low dose of **4c**, high and middle dose of **4e**, high dose of **4g**, low dose of **4h,** and low dose of **4i** were significantly different from those before administration, and higher than those before administration. The ratio of **4b** medium dose and **4f** high dose to sinomenine was significantly different and better than that of sinomenine. **4a**, **4b**, **and 4f** high and low dose, **4c and 4d** high and low dose, **4e** high and medium dose, **4g** high dose, **and 4h**, **4i** medium and low dose were significantly different from the blank group and higher than the blank group. The high dose of **4b** showed better than the blank group and the sinomenine group at 60 min, which was also significantly different from that before administration. The high dose of **4f** was better than that of the blank group and the sinomenine group at 15 min, 30 min, and 60 min, which was also significantly different from that before administration, indicating that it may have a significant analgesic effect.

Acetic acid-induced writhing test

The results of acetic acid-induced writhing test are shown in **Table 4**. At the dose of 30 mg/kg, the writhing latency, inhibition rate of writhing times, and percentage of analgesia of **4a**, **4d**, **4b**, **4e,** and **4g** were higher than those of sinomenine. The latent inhibition rate of other derivatives at each concentration (except for **4c** medium dose) was higher than that of the normal saline group. The reason why the latency of writhing, the inhibition rate of writhing times, and the percentage of analgesia in each dose of the same derivative were significantly different may be related to the individual differences in mice.

EXPERIMENTAL

Drugs and reagents

sinomenine hydrochloride, Lot No. C15533222, Shanghai McLean Biochemical Technology Co. Ltd; p-Bromobenzoic acid, Lot No.Lf1025177438, Shanghai Haohong Bio-medical Technology Co. Ltd; Dimethoxypyridine, Lot No. RH626903, Shanghai Een Chemical Technology Co. Ltd; all other reagents were obtained from Shanghai Titan Technology Co. SPF grade Kunming mice (SCXK [Xiang] 2019–0011), female, body mass (20 ± 4 g).

Instruments and consumables

The product mixtures were analyzed using fluorescent indicator thin layer chromatography plates provided by Yantai Jiangyou Silica Gel Co. The ultraviolet (UV)-active compounds were detected using a WD-9403A UV instrument (Beijing, China) (λ = 254 nm, 365 nm). Silica gel with particle size of 300–400 mesh was used as a stationary phase for column chromatography. The ^{1}H-NMR and ^{13}C-NMR spectra were obtained with a Bruker Avance 400 MHz NMR spectrometer at 400 MHz, respectively. The deuterated reagent peaks were analyzed with deuterated chloroform (^{1}H-NMR δ = 7.26 ppm, ^{13}C-NMR δ = 77.16 ppm) in ^{1}H and ^{13}C NMR analysis of the internal standard. Chemical shift values are expressed in parts per million (ppm), spin-spin coupling constants in hertz (Hz), and multiplicities are abbreviated as s (singlet), d (doublet), t (triplet), q (quadruplet), and m (multiplet). Q-Exactive Orbitrap MS (Thermo Fisher Scientific, Bremen, Germany) equipped with an electrospray ionization source. Pain thresholds of mice were monitored using the ZH-YLS-6BS intelligent hot plate instrument.

Molecular docking test

Nine sinomenine derivatives were docked with GBP5 protein (PDB no. 7ckf), using the molecular docking software MOE, with the binding site of GDP set as the docking pocket and one strand of the protein retained for docking.

Druggability analysis

Tencent AI Lab-iDrug platform was applied to predict the absorption distribution metabolism and drug formation of 4a-4i *in vivo*.

Procedures for the synthesis of sinomenine derivatives

Sinomenine (2)

Sinomenine hydrochloride 34.1 mmol (12.5 g) was dissolved in 100 mL distilled water, and then 5% NaOH

Table 2: Analysis of druggability of sinomenine and sinomenine derivatives

Drug	ClogP	Oral bioavailability (%)	Plasma protein binding ratio (%)	BBBP	Blood brain ratio	CYP induction probability	Human clearance	DILI
Sinomenine	2.02	20	53	0.98	−0.23	0.16	1.14	0.17
4a	4.29	39	87	0.84	0.64	0.15	1.2	0.28
4b	4.3	35	89	0.79	0.59	0.14	1.19	0.34
4c	4.3	36	83	0.64	0.59	0.15	1.23	0.3
4d	5.06	38	89	0.85	0.68	0.14	1.14	0.32
4e	5.06	38	86	0.85	0.66	0.13	1.08	0.32
4f	4.95	43	89	0.78	0.67	0.13	1.13	0.39
4g	4.95	45	89	0.77	0.68	0.14	1.06	0.42
4h	4.2	33	85	0.51	0.25	0.14	1.08	0.35
4i	4.2	32	89	0.61	0.19	0.12	0.97	0.43

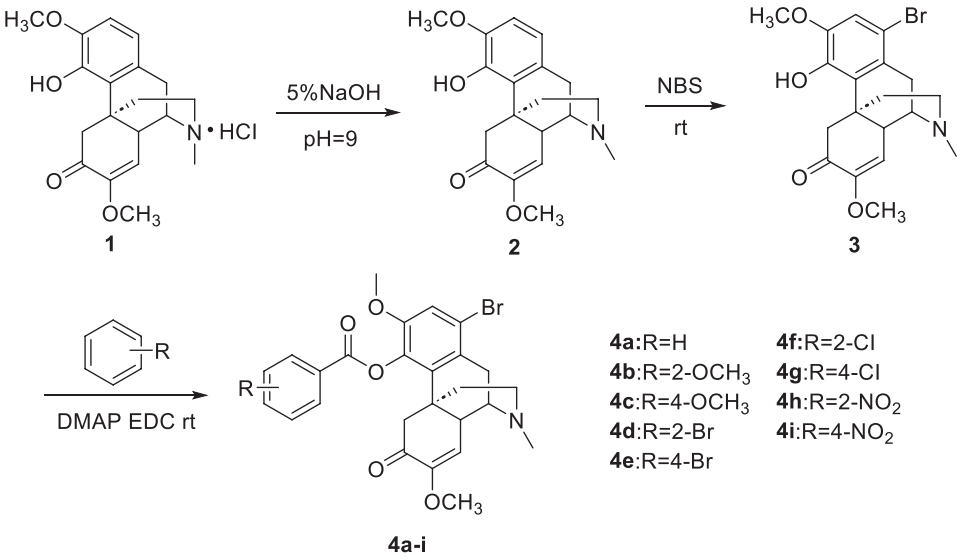

Scheme 2: Synthetic route for sinomenine derivatives 4a-i

was added to adjust the pH to 9.00. The turbid liquid was put into a 250 mL funnel, and 30 mL CH_2Cl_2 (DCM) was added. The organic phase was extracted 3 times repeatedly. The organic phase was combined, dried, and concentrated to obtain sinomenine intermediate 2 (10 g, 30.3 mmol), mp 20–25°C, with a yield of 89%.

Sinomenine bromide (3)

2 (6.06 mmol, 2 g) was dissolved in 20 mL of DCM, and NBS (6.66 mmol, 1.2 g) was dissolved in DCM and slowly added to sinomenine. After stirring at room temperature for 12 h, saturated salt water was added. The water layer was extracted with DCM (3 × 20 mL), dried with anhydrous sodium sulfate, and the organic layer was merged. The organic layer was further dried with anhydrous sodium sulfate and concentrated under reduced pressure. The brownish red residue was dissolved in DCM, purified by silica gel column, and eluted with DCM-MeOH (30:1) to obtain the key intermediate **3**, which was a dark yellow powder, mp 20–25°C, with a yield of 85%.[17]

4a (Benzoate bromo sinomenine)

3 (0.6g, 1.47 mmol), benzoic acid (0.22 g, 1.76 mmol), EDC (0.46 g, 2.94 mmol), and DMAP (0.27 g, 2.21 mmol) were added to the round bottom flask, and then 10 mL DCM was added as solvent. After stirring at room temperature for 10 h, saturated salt water (3 × 10 mL) was added for extraction. The organic layer was dried by anhydrous sodium sulfate, concentrated under reduced pressure, and separated by column chromatography (DCM: MeOH = 50: 1) to obtain a white solid, mp 20–25°C, with a yield of 81%.[18]

Characterization data

3: Red solid, mp 20–25°C, 85% yield, ^{1}H NMR (400 MHz, *Chloroform-d*) δ 6.95 (s, 1H), 5.39 (d, *J*=2.1 Hz, 1H), 4.33 (d, *J*=15.6 Hz, 1H), 3.83 (s, 4H), 3.50 (s, 4H), 3.05 (d, *J*= 19.3 Hz, 1H), 2.93 (s, 1H), 2.75 (dd, *J* = 19.4, 5.9 Hz, 1H), 2.65 (d, *J*=2.2 Hz, 3H), 2.55 (d, *J*=15.8 Hz, 1H), and 2.26 (td, *J*=13.9, 13.5, 6.6 Hz, 2H). ^{13}C NMR (101MHz, *Chloroform-d*) δ 193.74, 152.35, 145.75, 144.31, 129.09,

Table 3: Results of hot plate method for sinomenine and sinomenine derivatives

Compds	Dose (mg/kg)	Pain threshold before administration $\bar{X}$±s (s)	Pain threshold at different times after administration (s)		
			15 min	30 min	60 min
Sinomenine	15	9.91±2.62	10.39±3.26▲	11.63±2.36★▲	10.72±3.07
4a$_{C1}$	30	13.97±3.59	15.95±3.61 Δ ▲	14.56±4.13▲	13.32±3.41▲
4a$_{C2}$	15	10.58±2.27	13.77±3.43▲	11.37±2.25▲	11.97±3.44▲
4a$_{C3}$	7.5	8.19±2.09	7.25±1.12 Δ	10.63±1.91★▲	12.14±3.51★▲
4b$_{C1}$	30	9.57±3.26	13.97±3.03★▲	8.57±0.90 Δ	14.20±2.52★▲Δ
4b$_{C2}$	15	7.80±1.18	9.90±1.37★▲	14.30±3.13★▲	13.17±3.94▲★
4b$_{C3}$	7.5	8.43±2.73	9.52±2.87★	10.86±4.35★▲	9.71±2.16
4c$_{C1}$	30	10.80±2.51	11.42±4.68	14.26±4.12▲	14.40±4.25★▲
4c$_{C2}$	15	8.91±3.41	9.46±4.63	8.67±1.43 Δ	12.10±4.04
4c$_{C3}$	7.5	7.53±1.45	11.30±5.04★▲	10.90±3.10★▲	10.71±3.14★
4d$_{C1}$	30	11.92±3.74	11.05±4.22	13.64±4.57★▲	10.21±3.49
4d$_{C2}$	15	9.44±4.06	10.97±3.69	10.80±4.07★	10.38±4.61
4d$_{C3}$	7.5	9.20±2.75	13.40±2.70★▲	13.80±3.42▲	9.80±5.54
4e$_{C1}$	30	6.97±1.64	8.51±3.25	10.54±3.35★▲	12.31±2.82★▲
4e$_{C2}$	15	6.45±1.26	10.41±3.93★▲	6.81±2.00Δ	10.03±6.89★
4e$_{C3}$	7.5	6.02±0.81	5.96±1.78 Δ	7.75±3.75Δ	5.97±0.80★▲ Δ
4f$_{C1}$	30	10.57±1.47	16.33±3.93★▲Δ	16.11±3.40★▲Δ	16.74±2.83★▲Δ
4f$_{C2}$	15	9.68±2.43	12.86±2.56★▲	14.19±3.82★▲	13.14±4.00★▲
4f$_{C3}$	7.5	6.64±1.50	7.22±2.19	9.19±2.43★	10.59±1.90★▲
4g$_{C1}$	30	7.90±2.50	13.80±4.07★▲	8.40±2.72 Δ	7.96±2.45
4g$_{C2}$	15	8.90±3.50	7.61±1.75	9.75±4.86	8.90±3.34
4g$_{C3}$	7.5	10.43±4.15	12.44±5.35	9.73±3.50	10.26±4.20
4h$_{C1}$	30	7.93±1.94	8.55±2.27	6.03±3.55 Δ	7.89±3.02Δ
4h$_{C2}$	15	11.10±4.26	12.81±5.31★▲	13.23±4.03★▲	13.92±6.13★
4h$_{C3}$	7.5	10.50±3.38	12.94±4.26★▲	12.86±3.78★▲	14.42±3.61▲
4i$_{C1}$	30	7.06±1.89	8.35±1.43	8.34±3.20	8.06±1.90
4i$_{C2}$	15	12.94±1.14	9.94±1.74★	13.13±4.33▲	11.19±4.63
4i$_{C3}$	7.5	6.06±2.09	8.73±3.56★	10.34±2.00★▲	8.58±4.43★
blank		7.70±1.56	7.53±1.59	7.07±1.65	8.26±1.79

★, $P<0.05$ compared with pain threshold before administration; ▲, $P<0.05$ compared with blank; Δ, $P<0.05$ compared with Sinomenine group. Results are expressed as means±standard deviation (n=10 per group)

124.68, 114.78, 113.14, 112.94, 56.34, 56.12, 54.89, 48.97, 46.94, 45.59. 42.76, 41.06, 35.59, 26.04. HRMS (ESI) *m/z* calcd for $C_{19}H_{23}BrNO_4$+[M+H]+ 408.08049.

4a: White solid, mp 20–25°C, 81% yield, ^{1}H NMR (400 MHz, *Chloroform-d*) δ 8.35–8.29 (m, 2H), 7.67–7.61 (m, 1H), 7.55 (dd, *J*=8.4, 7.0 Hz, 2H), 7.07 (s, 1H), 5.46 (d, *J*=2.1 Hz, 1H), 3.89 (dd, *J*=15.8, 1.8 Hz, 1H), 3.66 (s, 3H), 3.49 (s, 3H), 3.26–3.21 (m, 1H), 3.10–2.96 (m, 2H), 2.52 (dd, *J*=9.6, 4.1 Hz, 1H), 2.50–2.44 (m, 2H), 2.42 (s, 3H), 2.12 (td, *J*=12.4, 3.4 Hz, 1H), 1.80 (td, *J*=12.6, 4.7 Hz, 1H), 1.63–1.56 (m, 1H). ^{13}C NMR (101 MHz, *Chloroform-d*) δ 192.39, 164.34, 152.74, 139.08, 133.91, 132.50, 130.81, 128.91, 128.87, 121.20, 115.27, 114.67, 112.12, 56.23. 56.21, 55.84, 55.03, 50.47, 46.38, 46.15, 46.13, 42.86, 41.49, 37.03, 26.20, 23.04. HRMS (ESI) *m/z* calcd for$C_{26}H_{27}O_5NBr$,[M+H]+ 512.10671.

4b: White solid, mp 20–25°C, 83% yield, ^{1}H NMR (400 MHz, *Chloroform-d*) δ 8.21 (d, *J*=7.7 Hz, 1H), 7.59–7.50 (m, 1H), 7.08 (d, *J*=7.6 Hz, 1H), 7.05 (d, *J*=2.9 Hz, 1H), 7.02 (d, *J*=8.6 Hz, 1H), 5.44 (d, *J*=2.1 Hz, 1H), 4.12 (d, *J*=16.2 Hz, 1H), 3.96 (s, 3H), 3.67 (s, 3H), 3.48 (s, 3H), 3.24 (t, *J*=4.7 Hz, 1H), 3.08–2.95 (m, 2H), 2.57–2.48 (m, 2H), 2.42 (s, 4H), 2.11 (td, *J*=12.3, 3.5 Hz, 1H), 1.81 (td, *J*=12.4, 4.4 Hz, 1H), 1.72 (d, *J*=12.8 Hz, 1H). ^{13}C NMR (101 MHz, *Chloroform-d*) δ 192.31, 163.28, 152.65, 150.14, 139.01, 134.82, 133.62, 132.92, 132.57, 130.11, 129.15, 127.83, 122.90, 121.36. 115.26, 114.72, 112.11, 56.26, 56.24, 55.86, 55.03, 50.24, 46.52, 45.97, 42.88, 41.41, 37.00, 26.24, 23.07. HRMS (ESI) *m/z* calcd for $C_{27}H_{29}O_6NBr$+[M+H] + 542.11682.

4c: White solid, mp 20–25°C, 82% yield, ^{1}H NMR (400 MHz, *Chloroform-d*) δ 8.32–8.24 (m, 2H), 7.05 (ddd, *J*=10.8, 6.2, 2.4 Hz, 9H), 5.47 (d, *J*=2.7 Hz, 1H), 3.95–3.86 (m, 4H), 3.68 (d, *J*=3.0 Hz, 9H), 3.50 (d, *J*=3.0 Hz, 9H), 3.50 (d, *J*=3.0 Hz, 9H) 1H), 3.95–3.86 (m, 4H), 3.68 (d, *J*=3.0 Hz, 9H), 3.50 (d, *J*=3.0 Hz, 3H), 3.26 (q, *J*=4.1 Hz, 1H), 3.07 (d, *J*=18.1 Hz, 1H), 2.99 (s, 1H), 2.63–2.32 (m, 20H), 2.14 (tt,

Table 4: Results of acetic acid-induced writhing test for sinomenine and sinomenine derivatives

Compds	Dose (mg/kg)	The prolonged rate of latency (%)	Writhing times inhibition rate (%)	Percentage of analgesia (%)
Sinomenine	15	39.1045	29.47	0
4a$_{C1}$	30	81.6273	74.88	20
4a$_{C2}$	15	50.1435	31.88	0
4a$_{C3}$	7.5	30.6087	26.09	0
4b$_{C1}$	30	69.9037	48.79	0
4b$_{C2}$	15	80.0805	69.08	20
4b$_{C3}$	7.5	20.3907	40.10	0
4c$_{C1}$	30	32.9706	60.87	0
4c$_{C2}$	15	15.4348	56.52	20
4c$_{C3}$	7.5	97.6221	76.81	60
4d$_{C1}$	30	82.2575	63.77	20
4d$_{C2}$	15	35.7901	28.50	0
4d$_{C3}$	7.5	73.6988	41.06	0
4e$_{C1}$	30	93.3893	64.73	20
4e$_{C2}$	15	30.4201	56.52	0
4e$_{C3}$	7.5	34.0270	51.69	0
4f$_{C1}$	30	25.8430	21.74	0
4f$_{C2}$	15	43.2262	55.31	0
4f$_{C3}$	7.5	56.6589	42.03	0
4g$_{C1}$	30	88.9405	50.24	20
4g$_{C2}$	15	42.7349	43.42	0
4g$_{C3}$	7.5	17.7092	37.20	0
4h$_{C1}$	30	62.8503	75.85	0
4h$_{C2}$	15	79.5584	73.43	0
4h$_{C3}$	7.5	59.4140	60.87	0
4i$_{C1}$	30	53.7499	28.02	0
4i$_{C2}$	15	26.3882	27.54	0
4i$_{C3}$	7.5	21.9993	25.12	0
Saline		18.1006		0

J=12.4, 3.4 Hz, 1H), 1.81 (tt, *J*=12.7, 3.9 Hz, 1H), 1.66–1.57 (m, 3H). ^{13}C NMR (101 MHz, *Chloroform-d*) δ 192.50, 164.23, 164.07, 152.79, 150.51, 133.03, 132.55, 128.93, 121.24, 121.07, 115.28, 114.67, 114.24, 56.28. 55.68, 55.08, 50.54, 46.44, 46.19, 42.89, 41.52, 37.04, 26.24. HRMS (ESI) *m/z* calcd for $C_{27}H_{29}O_6NBr$+[M+H]+ 542.11727.

4d: White solid, mp 20–25°C, 82% yield, ^{1}H NMR (400 MHz, *Chloroform-d*) δ 8.28 (d, *J*=7.7 Hz, 1H), 7.72 (dd, *J*=8.0, 1.2 Hz, 1H), 7.49 (t, *J*=7.6 Hz, 1H), 7.41 (td, *J*=7.7, 1.8 Hz, 1H), 7.08 (s, 1H), 5.45 (d, *J*=2.2 Hz, 1H), 3.80 (d, *J*=15.9 Hz, 1H), 3.71 (s, 3H), 3.48 (s, 3H), 3.24 (q, *J*=5.0 Hz, 1H), 3.09–2.93 (m, 2H), 2.57–2.51 (m 2H), 2.48 (d, *J*=6.7 Hz, 1H), 2.43 (s, 3H), 2.13 (t, *J*=12.4 Hz, 1H), 1.86 (td, *J*=12.5, 4.5 Hz, 1H), 1.75 (d, *J*=12.9 Hz, 1H). ^{13}C NMR (101 MHz, *Chloroform-d*) δ 192.55, 163.54, 160.42, 152.64, 150.41, 139.43, 134.85, 133.48, 128.93, 120.88, 120.53, 117.95, 115.22, 114.64. 112.24, 56.29, 56.00, 55.92, 54.99, 49.72, 49.68, 46.63, 45.86, 42.83, 41.18, 36.91, 26.25, 23.08. HRMS (ESI) *m/z* calcd for $C_{26}H_{26}O_5NBr$ [81] Br+[M+H]+ 592.01517.

4e: White solid, mp 20–25°C, 82% yield, ^{1}H NMR (400 MHz, *Chloroform-d*) δ 8.19 (d, *J*=8.3 Hz, 2H), 7.70 (d, *J*=8.5 Hz, 2H), 7.08 (s, 1H), 5.46 (d, *J*=2.1 Hz, 1H), 3.80 (d, *J*=15.7 Hz, 1H), 3.50 (s, 3H), 3.24 (t, *J*=4.8 Hz, 1H), 3.12–2.96 (m, 2H), 2.13 (td, *J*=12.5, 3.4 Hz, 1H), 1.81 (dd, *J*=12.6, 4.6 Hz, 1H), 1.57 (d, *J*=12.8 Hz, 1H). ^{13}C NMR (101 MHz, *Chloroform-d*) δ 192.39, 163.72, 152.81, 150.19, 132.36, 129.39, 129.11, 121.40, 115.32, 114.70, 112.17, 56.24, 55.09, 50.67, 46.35, 42.92, 41.60, 37.13, 26.24, 23.07. HRMS (ESI) *m/z* calcd for $C_{26}H_{26}O_5NBr$ [81] Br+[M+H]+ 592.01351.

4f: White solid, mp 20–25°C, 82% yield, ^{1}H NMR (400 MHz, *Chloroform-d*) δ 8.29 (d, *J*=7.6 Hz, 1H), 7.53–7.48 (m, 2H), 7.48–7.41 (m, 1H), 7.08 (s, 1H), 5.45 (d, *J*=2.1 Hz, 1H), 3.81 (d, *J*=16.0 Hz, 1H), 3.71 (s, 3H), 3.48 (s, 3H), 3.24 (d, *J*=9.3 Hz, 1H), 3.10–2.94 (m, 2H), 2.57–2.51 (m, 1H), 2.50–2.45 (m, 1H), 2.43 (s, 4H), 2.43 (m, 4H), 2.50–2.45 (m, 1H), 2.50–2.45 (m, 1H), 2.50–2.45 (m, 1H), 2.50–2.45 (m, 1H) 2.43 (s, 4H), 2.11 (d, *J*=13.7 Hz, 1H), 1.85 (td, *J*=12.5,4.6 Hz, 1H), 1.72 (d, *J*=12.8 Hz, 1H). ^{13}C

NMR (101 MHz, *Chloroform-d*) δ 192.33, 162.74, 152.66, 150.15, 139.00, 134.95, 133.59, 132.86, 131.45, 129.15, 128.22, 127.24, 121.33, 115.27. 114.73, 112.12, 56.27, 56.23, 55.85, 55.02, 50.27, 50.23, 46.50, 45.97, 42.87, 41.40, 41.23, 36.99, 26.24, 23.07. HRMS (ESI) *m/z* calcd for $C_{26}H_{26}O_5NBrCl$+[M+H]+ 546.06773.

4g: White solid, mp 20–25°C, 80% yield, ^{1}H NMR (400 MHz, *Chloroform-d*) δ 8.27 (d, *J*=8.4 Hz, 2H), 7.53 (d, *J*=8.6 Hz, 2H), 7.08 (s, 1H), 5.47 (d, *J*=2.1 Hz, 3H), 3.80 (dd, *J*=15.6, 1.9 Hz, 1H), 3.68 (s, 3H), 3.50 (s, 3H), 3.29–3.18 (m, 4H), 3.12–2.91 (m, 8H), 2.57–2.44 (m, 9H), 2.44 (s, 4H), 2.12 (td, *J*=12.3, 3.4 Hz, 4H), 1.82 (td, *J*=12.6, 4.7 Hz, 3H), 1.57 (dt, *J*=12.7, 2.6 Hz, 3H). ^{13}C NMR (101 MHz, *Chloroform-d*) δ 192.43, 163.58, 152.81, 150.21, 140.62, 138.89, 132.50, 132.27, 129.35, 129.12, 127.36, 121.40, 115.31, 114.71. 112.16, 56.27, 56.22, 55.85, 55.10, 50.67, 46.34, 46.27, 42.92, 41.61, 41.43, 37.15, 26.23, 23.06. HRMS (ESI) *m/z* calcd for $C_{26}H_{26}O_5NBrCl$+[M+H]+ 546.06773.

4h: Yellow solid, mp 20–25°C, 80% yield, ^{1}H NMR (400 MHz, *Chloroform-d*) δ 8.52 (d, *J*=8.6 Hz, 2H), 8.41 (d, *J*=8.6 Hz, 2H), 7.10 (s, 1H), 5.48 (d, *J*=2.1 Hz, 1H), 3.73 (d, *J*=15.3 Hz, 1H), 3.69 (s, 2H), 3.51 (s, 3H), 3.26 (t, *J* = 4.8 Hz, 1H), 3.13–2.99 (m, 2H), 2.52 (dq, *J*=13.7, 6.0, 5.2 Hz, 3H), 2.45 (s, 3H), 2.14 (td, *J*=12.4, 3.4 Hz, 1H), 1.85 (td, *J*=12.5, 4.6 Hz, 1H), 1.55 (d, *J*=12.6 Hz, 1H). ^{13}C NMR (101MHz, *Chloroform-d*) δ 192.40, 162.62, 152.81, 151.17, 149.87, 138.56, 134.19, 132.40, 132.08, 131.63, 129.22, 124.11, 123.95, 121.78. 115.33, 114.68, 112.18, 56.28, 56.16, 55.79, 55.14, 50.84, 46.29, 46.26, 42.96, 41.68, 37.24, 26.20, 23.02. HRMS (ESI) *m/z* calcd for $C_{26}H_{26}O_7N_2Br$+[M+H]+ 557.09179.

4i: Yellow solid, mp 20–25°C, 81% yield, ^{1}H NMR (400 MHz, *Chloroform-d*) δ 8.18 (d, *J*=7.5 Hz, 1H), 7.92 (d, *J*=7.9 Hz, 1H), 7.74 (dt, *J*=25.1, 7.6 Hz, 2H), 7.10 (s, 1H), 5.47 (s, 1H), 3.89 (d, *J*=16.4 Hz, 1H), 3.77 (s, 3H), 3.49 (s, 3H), 3.25 (t, *J*=4.7 Hz, 1H), 3.09 (dd, *J*=18.9, 14.6 Hz, 1H), 3.02 (s, 1H), 2.63–2.50 (m, 2H), 2.47 (d, *J*=19.3 Hz, 4H), 2.10 (d, *J*=9.2 Hz, 1H), 1.96 (q, *J*=4.1, 3.5 Hz, 2H). ^{13}C NMR (101MHz, *Chloroform-d*) δ 192.59, 162.75, 152.63, 149.90, 148.80, 133.20, 133.01, 132.68, 131.20, 129.49, 124.13, 121.81, 115.28, 114.94. 112.13, 56.28, 56.24, 55.06, 50.14, 46.51, 46.01, 42.94, 41.65, 36.85, 26.29, 23.10. HRMS (ESI) *m/z* calcd for $C_{26}H_{26}O_7N_2Br$+[M+H]+ 557.09179.

Bioassay for *in vivo* analgesic activity

Hot plate method

According to the hot plate method in the literature,[19] the mice were placed on a hot plate with a cut-off time of 30s to avoid damaging the claws of the animals. The mice were randomly divided into 29 groups, 10 mice in each group. The mice in the blank group were intragastrically administered with the same dose of normal saline, the sinomenine group was intragastrically administered with 15 mg/kg of sinomenine, and the experimental group was intragastrically administered with various doses of derivatives (7.5 mg/kg in the low dose group, 15 mg/kg in the middle dose group, and 30 mg/kg in the high dose group). Gavage for 3 days. After the last administration, the mice were recorded 15 min, 30 min, and 60 min licking hind foot time, as the reaction time (pain threshold).

Acetic acid-induced writhing test

According to the acetic acid-induced writhing test,[20] Young Kunming mice were intraperitoneally injected with 0.6% acetic acid at a dose of 0.1 mL/kg before administration (10 mice in each group). Record the first writhing time (latency period). Then, the sinomenine (15 mg/kg), normal saline (10 mL/kg), and various doses of derivatives (7.5 mg/kg in the low dose group, 15 mg/kg in the middle dose group, and 30 mg/kg in the high dose group) were administered orally 3 days (1 day a time) before treatment with acetic acid. Half an hour after the last administration, the mice were intraperitoneally injected with 0.6% acetic acid. The first writhing time and the number of writhing in 15 min were observed and recorded immediately.

The prolonged rate of latency (%) = (time after administration-time before administration)/time before administration × 100%.

Percentage of analgesia (%) = (number of twisted rats in control group-number of twisted rats in the experimental group)/number of twisted rats in control group × 100%.

Writhing times inhibition rate (%) = (mean number of torsion body in the control group-mean number of torsion body in the experimental group)/mean number of torsion in the control group × 100%.

Statistical analysis

Results were analyzed using Statistical Package for the Social Sciences 20.0. Multiple comparisons were performed using one-way analysis of variance, followed by least significant difference *t*-test. Results were considered statistically significant with a $P < 0.05$. Results are expressed as mean ± standard deviation.

CONCLUSION

In this work, we designed and synthesized nine sinomenine derivatives. Molecular docking software MOE was used. The target protein was GBP5 protein reported in the literature, and the binding site of GDP was set as the docking pocket. The results showed that all derivatives had good binding activity with the target protein. The Tencent AI Lab-iDrug platform was used to pre-prepare the druggability of the derivatives by computer-aided method. The results showed that each derivative had similar druggability to sinomenine. The analgesic activities of all compounds were evaluated by the hot plate method and acetic acid writhing method. The results of hot plate method showed that the synthesized compounds had certain analgesic effects, and the analgesic effects of two compounds were better. The results of acetic acid writhing test showed that the synthesized compounds had a certain analgesic effect. The analgesic effect of **4a, 4b, 4d, 4e,** and **4g** was better than that of sinomenine, and the other derivatives were equivalent to that of sinomenine.

FUNDING

This research was funded by Hunan natural science foundation Program Project (grant no.2023JJ50462) and the Huaihua University Program (grant no.SWGC-02).

REFERENCES

[1] Zhao, X., Peng, C., Zhang, H. and Qin, L. *Sinomenium acutum*: A review of chemistry, pharmacology, pharmacokinetics, and clinical use, *Pharm. Biol*., **2012**, *50*, 1053–1061. doi: 10.3109/13880209.2012.656847

[2] Chopra, A. and Abdel-Nasser, A. Epidemiology of rheumatic musculoskeletal disorders in the developing world, *Best Pract. Res. Clin. Rheumatol*., **2008**, *22*, 583–604. doi: 10.1016/j.berh.2008.07.001

[3] Li, S. *Compendium of Materia Medica*. Beijing: Beijing People's Publishing House, **1997**, p31340.

[4] Huang, Z., Mao, X., Chen, J., He, J., Shi, S., Gui, M., Gao, H. and Hong, Z. The Efficacy and safety of zhengqing fengtongning for knee osteoarthritis: A systematic review and meta-analysis of randomized clinical trials, *Evid. Based Complement. Alt*., **2022**, *2022*, 2768444. doi: 10.1155/2022/2768444

[5] Li, Q., Zhou, W., Wang, Y., Kou, F., Lyu, C. and Wei, H. Metabolic mechanism and anti-inflammation effects of sinomenine and its major metabolites N-demethylsinomenine and sinomenine-N-oxide, *Life Sci*., **2020**, *261*, 118433. doi: 10.1016/j.lfs.2020.118433

[6] Gao, T., Hao, J., Wiesenfeld-Hallin, Z., Wang, D.Q. and Xu, X.J. Analgesic effect of sinomenine in rodents after inflammation and nerve injury, *Eur. J. Pharmacol*., **2013**, *721*, 5–11. doi: 10.1016/j.ejphar.2013.09.062

[7] Wang, Q. and Li, X. Immunosuppressive and anti-inflammatory activities of sinomenine, *Int. Immunopharmacol*., **2011**, *11*, 373–376. doi: 10.1016/j.intimp.2010.11.018

[8] Zhang, W., Gao, Y., Yang, N., Zhang, H., Zhang, F., Chen, H.Q., Meng, J., Zhang, S. and Li, W. Sinomenine-loaded microcapsules fabricated by phase reversion emulsification-drying in liquid method: An evaluation of process parameters, characterization, and released properties, *J. Bioact. Compat. Pol*., **2018**, *33*, 382–396. doi: 10.1177/0883911517751159

[9] Lin, Y., Yi, O., Hu, M., Hu, S., Su, Z., Liao, J., Wang, W., Wang, S., Liu, L., Liu, B. and Cai, X. Multifunctional nanoparticles of sinomenine hydrochloride for treat-to-target therapy of rheumatoid arthritis via modulation of proinflammatory cytokines, *J. Control. Release*, **2022**, *348*, 42–56. doi: 10.1016/j.jconrel.2022.05.016

[10] Wu, S., Zeng, Q., Zhang, Z., Zhang, X., Hou, Y., Li, Z., Jia, C., Liu, Y. and Li, W. Development of sinomenine hydrochloride sustained-release pellet using a novel whirlwind fluidized bed, *J. Drug Deliv. Sci. Tec*., **2022**, *78*, 103956. doi: 10.1016/j.jddst.2022.103956

[11] Li, S., Gao, M., Nian, X., Zhang, L., Li, J., Cui, D., Zhang, C. and Zhao, C. Design, synthesis, biological evaluation and silico prediction of novel sinomenine derivatives, *Molecules*, **2021**, *26*, 3466. doi: 10.3390/molecules26113466

[12] Zheng, H., Xu, C., Fei, Y., Wang, J., Yang, M., Fang, L., Wei, Y., Mu, C., Sheng, Y., Li, F., Zhu, J. and Tao, C. Monoterpenes-containing PEGylated transfersomes for enhancing joint cavity drug delivery evidenced by CLSM and double-sited microdialysis, *Mat. Sci. Eng. C*, **2020**, *113*, 110929. doi: 10.1016/j.msec.2020.110929

[13] Zhao, L., Zhang, M., Liu, Y., Tan, Y., Yin, J., Chen, Y., Chen, D. and Ni, B. Sinomenine alleviates lipopolysaccharide-induced acute lung injury via a PPARβ/δ-dependent mechanism, *Eur. J. Pharmacol*., **2023**, *953*, 175838. doi: 10.1016/j.ejphar.2023.175838

[14] Ni, P., Liu, Y., Man, J., Li, W., Xue, S., Lu, T., Su, Z. and Zhou, C. C16, a novel sinomenine derivatives, promoted macrophage reprogramming toward M2-like phenotype and protected mice from endotoxemia, *Int. J. Immunopath. Pharmacol*., **2021**, *35*, 1-9. doi: 10.1177/20587384211026786

[15] Li, J., Deng, H., Yao, Y., Wang, W., Hu, J., Dong, Y., Wang, P., Liu, L., Liu, Z., Xie, Y., Li, L. and Zhou, H. Sinomenine ameliorates collagen-induced arthritis in mice by targeting GBP5 and regulating the P2X7 receptor to suppress NLRP3-related signaling pathways, *Acta Pharmacol. Sin*., **2023**, *44*, 2504–2524. doi: 10.1038/s41401-023-01124-4

[16] Zhao, Z., Xiao, J., Wang, J., Dong, W., Peng, Z. and An, D. Anti-inflammatory effects of novel sinomenine derivatives, *Int. Immunopharmacol*., **2015**, *29*, 354–360. doi: 10.1016/j.intimp.2015.10.030

[17] Gao, F., Dai, Z., Zhang, T., Gu, Y., Cai, D., Lu, M., Zhang, Z., Zeng, Q., Shang, B., Xu, B. and Lei, H. Synthesis and biological evaluation of novel sinomenine derivatives as anti-inflammatory and analgesic agent, *Rsc Adv.*, **2022**, *12*, 30001–30007. doi: 10.1039/D2RA05558A

[18] Zhang, Z., Wang, H., Yuan, J., Li, X., Fang, N., Lin, M., Hou, Q. and Ji, T. Design, synthesis, and pharmacological evaluation of sinomenine derivatives on rings A and C: Novel compounds screening for aplastic anemia targeting on cytotoxic T lymphocyte, *Eur. J. Med. Chem*., **2021**, *225*, 113791. doi: 10.1016/j.ejmech.2021.113791

[19] Da Costa, R.H.S., Martins, A.O.B.P.B., Pessoa, R.T., Alshehri, S.A., Wahab, S., Ahmad, M.F., Suliman, M., Da Silva, L.Y.S., Alcântara, I.S. and Ramos, A.G.B. Mechanisms of actions involved in the antinociceptive effect of estragole and its β-cyclodextrin inclusion complex in animal models, *Plants*, **2022**, *11*, 2854. doi: 10.3390/plants11212854

[20] Mazumder, T., Hasan, T., Ahmed, K.S., Hossain, H., Debnath, T., Jahan, E., Rahman, N., Shuvo, M.S.R. and Daula, A.S.U. Phenolic compounds and extracts from Crotalaria calycina Schrank potentially alleviate pain and inflammation through inhibition of cyclooxygenase-2: An *in vivo* and molecular dynamics studies, *Heliyon*, **2022**, *8*, e12368. doi: 10.1016/j.heliyon.2022.e12368

Received: 05 Jan 2023; Accepted: 11 Jan 2023

Indian Journal of Heterocyclic Chemistry
Vol. 35 - Number 02 (Apr-Jun 2025) 559-568
https://connectjournals.com/01951.2025.35.559
https://doi.org/10.59467/IJHC.2025.35.559

ISSN (Print) : 0971-1627
ISSN (Online) : 2456-4311

Toward the development of better therapeutic agents for *Mycobacterium Tuberculosis*: Computational design and evaluation of pyrazinone derivatives as inhibitors of enoyl acyl carrier protein reductase

Akshita Goel[1,2], Indu Negi[1], Sanchita Aggarwal[1], Ankur Ganesh Pandey[1]* and Purshotam Sharma[1]*

[1] Department of Chemistry and Centre of Advanced Studies in Chemistry, Panjab University, Chandigarh, India
[2] Chandigarh Group of Colleges, Jhanjheri, Mohali, Punjab, India

ABSTRACT The treatment of tuberculosis (TB) has become challenging, and efficient therapies need to be developed. Here, we apply *in silico* techniques to analyze the inhibitory role of pyrazinone derivatives toward enoyl-acyl carrier protein reductase (InhA) and compare our results with isoniazid, a well-known first-line TB drug. Docking suggests that despite binding within the same pocket, pyrazinone derivatives interact more strongly with InhA than isoniazid. Although C6 substitution does not significantly affect the ligand binding, N4-methoxybenzyl derivatives exhibit higher docking scores than their N4-ethyl counterparts. MD simulations suggest that the crucial interaction with Arg194 observed in the docked structures is mostly retained. In synchrony with MMGBSA binding energy calculations and QM calculations, analysis of the hydrogen bond occupancies and interaction energies reveal that pyrazinone derivatives with *N*4-methoxybenzyl substitution bind more strongly to InhA compared to *N*4-ethyl substituted derivatives. Our study thus identifies promising candidate compounds for potential inhibitory effects toward InhA.

KEY WORDS Enoyl acyl carrier protein reductase, Molecular docking, Molecular dynamics simulations, Quantum mechanical calculations, Tuberculosis.

How to cite this article: Goel, A., Negi, I., Aggarwal, S., Pandey, A.G., and Sharma, P. Toward the development of better therapeutic agents for *Mycobacterium Tuberculosis*: Computational design and evaluation of pyrazinone derivatives as inhibitors of enoyl acyl carrier protein reductase, *Indian J. Heterocycl. Chem.*, **2025**, *35*, 559–568. *https://doi.org/10.59467/IJHC.2025.35.559*

INTRODUCTION

Tuberculosis (TB) is an infection caused by *Mycobacterium tuberculosis* (*Mtb*), with potentially disastrous consequences for public health.[1] Specifically, TB is one of the top ten causes of death worldwide.[2] The Global Tuberculosis Report of 2021 points to the recent reversal in progress toward tackling TB, mainly due to the enhanced deployment of resources toward the management of the COVID-19 pandemic.[3] In fact, the data compiled during the COVID-19 era suggests that 1.4 million fewer people received care for TB in 2020 than in 2019, which could result in half a million TB deaths and translates to a setback in the timeline of TB control by a decade.[4] More importantly, TB-associated mortality is increasing despite the evolution of frontline anti-TB drugs (e.g., isoniazid, pyrazinamide [PZA], rifampin, and ethionamide [ETH]), mainly due to the length of treatment, cost-associated inaccessibility, evolution of drug-resistant *Mtb* strains,[5] and common side effects.[6] Thus, WHO's goal to decrease TB incidents and deaths by more than 90% in the coming years seems difficult to achieve without the discovery of new anti-TB drugs.[7]

Intrinsic resistance to general-purpose antibiotics is a serious problem with the infections caused by *Mtb*.[8] This mainly stems from the low permeability of the hydrophobic cell wall, which protects *Mtb* from the host immune system and reduces the permeability of many drugs.[9] This, in turn, allows the pathogen to proliferate and persist for extended periods in the infected host.[10] Mycolic acids are the major components of the *Mtb* cell wall and are responsible for its low permeability,[11] since they form a bilayer interleaved

*Corresponding authors: Email: apandey@pu.ac.in; psharma@pu.ac.in

Published & Hosted by :
Journal Homepage :
www.connectjournals.com/ijhc
www.connectjournals.com

with extremely hydrophobic phenolic glycolipids, which generate a waxy surface that prevents the cell from macrophages, antiseptics, and antibiotics.[12] Inhibition of mycolic acid biosynthesis can help produce imperfections in the *Mtb* cell wall and can thus be a promising strategy for the development of anti-TB drugs.

The biosynthesis of mycolic acids in *Mtb* is carried out by two fatty acid synthases (FASs) – the "eukaryotic-like" multifunctional FAS-I and the "bacterial-like" dissociated FAS-II. Although FAS-I produces C_{16}–C_{18} and C_{24}–C_{26} acids (the latter correspond to the α branch of mycolic acids), FAS-II elongates the medium chain fatty acids at the very origin of the long meromycolic chains,[13] which further undergo Claisen condensation with the α-branch produced by FAS-I to yield the characteristic 2-alkyl-3-hydroxy motif of mycolic acids.[14] Enoyl-acyl carrier protein reductase (InhA) is one of the essential *Mtb* FAS-II proteins,[15] which reduces the 2-trans-enoyl-acyl carrier protein by utilizing NADH during the elongation step of the FAS-II pathway.[16] Consequently, InhA is a popular target for the designing of new TB drugs.[17]

Mycolic acid synthesis has been the target of a few available TB drugs. Specifically, despite its remarkably complex mode of action,[18] isoniazid (isonicotinyl hydrazine), the first-line TB drug, was the first-ever compound shown to inhibit mycolic acid synthesis.[19] ETH, a prodrug and a structural analog of isoniazid, is a second-line TB drug that targets InhA.[20] However, both isoniazid and ETH produce severe side effects, which include gastrointestinal toxicity and hepatotoxicity, dermatological manifestations, and neuropsychiatric effects.[6] In addition, these drugs are resistant to the commonly isolated clinical *Mtb* strains.[21] However, a previous report has suggested that PZA, another first-line TB drug, a prodrug of pyrazinoic acid (POA)[22] and a nicotinamide analog, and an efficient inhibitor of ribosomal protein S1 of *Mtb*[23] can act as a potential inhibitor for pathways involving InhA.[24] Specifically, PZA plays a role in combating the deteriorating effects of TB, shortening the course of its treatment and the treatment of patients infected with isoniazid- and rifampicin-resistant strains.[25] However, several studies indicate that *Mtb* strains resistant to isoniazid are also resistant to PZA due to mutations in the target genes.[25-27]

Despite the limitations of PZA, other pyrazine derivatives, particularly 5(1*H*)-pyrazinones, possess a number of pharmacological characteristics, which include antibacterial, antifungal, anticancer, and antiviral properties.[28,29] Previously, substituted pyrazinones have been studied experimentally, some of which exhibit moderate inhibitory properties against *Mtb* (**Figure S1** [SI, https://doi.org/10.5281/zenodo.15537581]).[30] However, the inhibitory effects of pyrazinone derivatives against TB in general, and InhA in particular, have not been studied in detail in the literature. To fill this void, in the present work, we computationally design and test novel pyrazinone scaffolds and analyze their interaction with InhA. These substitutions on the pyrazinone skeleton were chosen to enhance its therapeutic applications. Specifically, to harness the known pharmacological and therapeutic activity of thiophene heterocycles,[31,32] we substituted (2- or 3-) thiophenyl group at the C6 position of the pyrazinone ring (compounds **I, II, V,** and **VI**, **Figure 1**). Analogs with C6-phenyl and chloro substitution were also designed (compounds **III, IV, VII,** and **VIII**, **Figure 1**) and analyzed for comparison. Further, in analogy with a previous study,[30] we substituted the ethyl

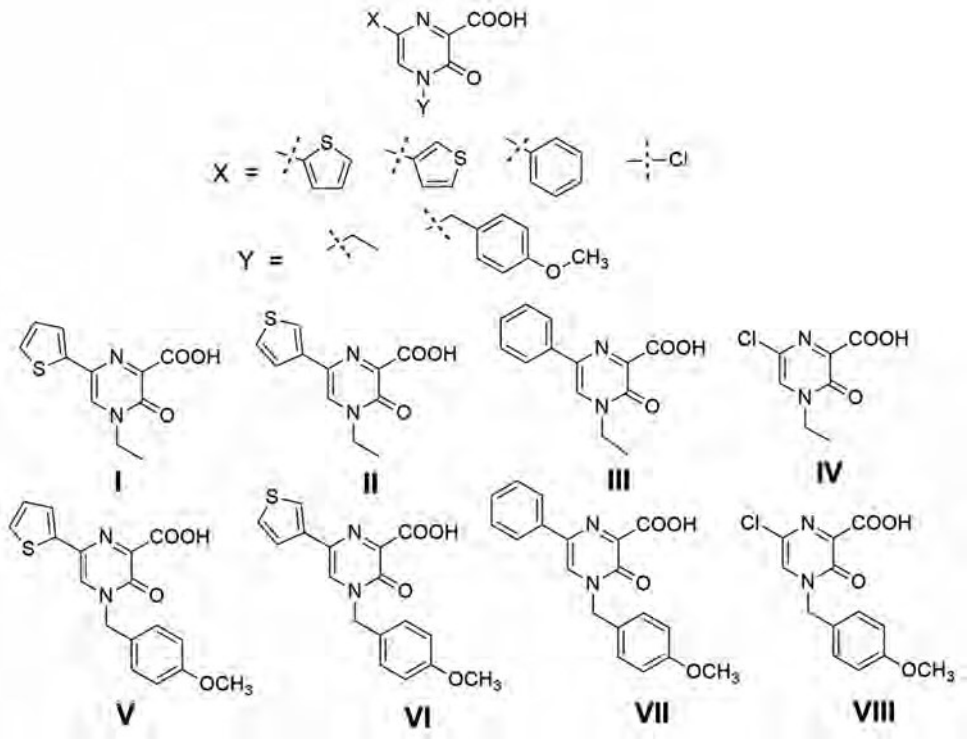

Figure 1: Structures of the pyrazinone derivatives analyzed in the present work

group at the N4 position of the pyrazine ring (compounds **I–IV**, **Figure 1**) and compared with the hydrophobic methoxybenzyl ether substitution (compounds **V–VIII**, **Figure 1**). All the analyzed compounds involve a carboxylate group at the C2 position that mimics the structure of POA.

We use virtual screening techniques, including molecular docking, molecular dynamics (MD) simulations, molecular mechanics generalized born surface area (MMGBSA) calculations, and quantum mechanical (QM) calculations to investigate the complexes of InhA and pyrazinone derivatives. In addition, we carried out a comparative analysis of the apo form of InhA to investigate the structural changes that occur in ligand binding. We further compared the ligand binding mode in our complexes with the complexes involving InhA and isoniazid, the well-known anti-TB drugs. Overall, the structure-based approach presented in this work will hopefully inspire future experimental and computational studies for designing better analogs to enhance the ligand interactions within the binding pocket of InhA and to discover and test new compounds for treating *Mtb* infection.

RESULTS AND DISCUSSION

Global receptor features do not significantly deviate in simulations of different holo states of InhA compared to the apo form

Comparison of the average backbone root-mean-square deviation (RMSD) values of the apo (3.3 Å) and ligand-bound (1–2 Å) forms of InhA obtained from simulations of the docked structures points to the structural stability acquired after ligand binding (**Figure 2B** and **Table S1** [SI, https://doi.org/10.5281/zenodo.15537581]), where all eight pyrazinone derivatives (**I–VIII**, **Figure 1**) provide greater stability to the receptor (average RMSD of 1.5 Å) compared to isoniazid (average RMSD of 2.0 Å, **Table S1**). More importantly, in all complexes, RMSD becomes uniform toward the end of the simulation (**Figures S2 and S3** [SI, https://doi.org/10.5281/zenodo.15537581]), which also correlates with the root-mean-square average correlation (RAC) values that approach zero toward the end of each simulation (**Figures 2A**, **S4 and S5** [SI, https://doi.org/10.5281/zenodo.15537581]), indicating structural convergence. Further, similar RoG values of the apo form (17.9 Å) and the ligand-bound forms (17.6 Å–18.3 Å) suggest that despite dynamic fluctuations in RoG values over the simulation time, ligand binding does not significantly perturb the overall InhA structure (**Table S2**, **Figures 2D** and **S6, S7** [SI, https://doi.org/10.5281/zenodo.15537581]). Furthermore, no significant differences are observed in the solvent-accessible surface area of the apo and ligand-bound forms of the protein (**Table S2**, **Figures 2E** and **S8, S9** [SI, https://doi.org/10.5281/zenodo.15537581]). Overall, this suggests that ligand-binding mostly affects the active site of InhA.

Change in flexibility within the InhA structure is significant in all the protein: ligand complexes compared to the apo form

Previous studies suggest that smaller scattering along the first two components obtained from principal component analysis (PCA) indicates the stable nature of the complex due to correlated motions.[33,34] On similar lines, PCA analysis of our simulated complexes suggests that the complexed protein is more compact as compared to the apoprotein (**Figures 3** and **S10–S12** [**SI**, https://doi.org/10.5281/zenodo.15537581]), thus revealing reduced flexibility within the ligand binding site. Further, the movement on the PCA2

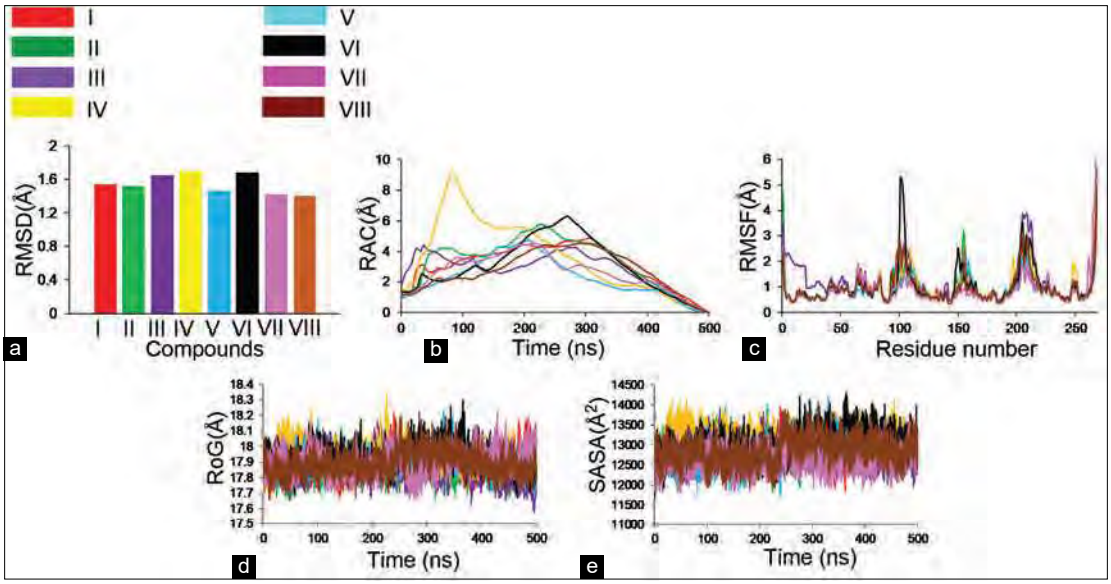

Figure 2: (a) Root-mean-square average correlation (RAC) values of molecular dynamics (MD) simulated complexes containing the carboxylate ionized form of the ligand as a function of the simulation time. (b) Root-mean-square deviation (RMSD) values of all protein backbone atoms of complexes with respect to the first simulation frame, as a function of the simulation time. (c) Root-mean-square fluctuation (RMSF) values of all Cα atoms of the complexes as a function of the simulation time. (d) Radius of gyration (RoG) values of the protein component of the complexes as a function of simulation time. (e) Solvent accessible surface area (SASA) values of the complexes as a function of simulation time

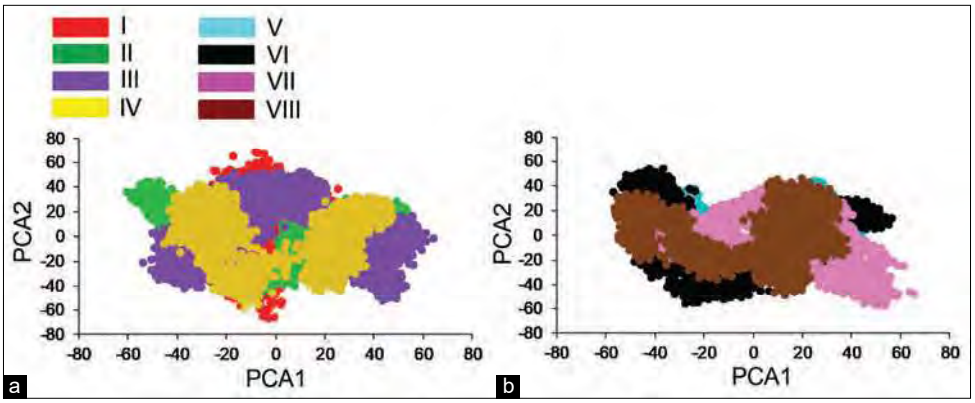

Figure 3: Principal component analysis (PCA) of the simulated complexes of InhA with the carboxylate-ionized form of (a) *N*4-ethyl substituted compounds (I–IV) and (b) *N*4-methoxybenzyl substituted compounds (V–VIII)

axis shows the negative loading (i.e., the scattering of dots [each dot shows the single conformation] is more toward the negative side of the vertical axis) compared to the apoprotein (**Figures 3** and **S10–S12**). This suggests that all the compounds (**I–VIII**) would cause reduced flexibility, resulting in inhibition of the target enzyme (**Figures S10–S12**).[33] Although the dynamics of PCs of all ligands are very similar, the close comparison reveals the greater movement of complexes containing pyrazinone derivatives toward the negative axis compared to isoniazid, indicating their higher inhibition potential (**Figures 3 and S12**). Further, among the pyrazinone derivatives, the movement along the PCA2 axis in *N*4-ethyl substituted ligands (**Figure 3 and S10**) is more toward the positive side in comparison to N4-methoxybenzyl substituted ligands (**Figures 3 and S11**). This indicates the better inhibition efficiency of the N4-methoxybenzyl substituted ligands towards InhA.

Root-mean-square fluctuations (RMSF) analysis reveals fluctuations at residues 100–120, 150–160, and 205–220 in the ligand-bound form as well as the apoprotein, although these fluctuations are comparatively less prominent in the ligand-bound protein (**Figures 2C**, **S13,** and **S14** [SI, https://doi.org/10.5281/zenodo.15537581]). Further, these fluctuations are reduced in complexes of pyrazinone derivatives compared to isoniazid, which further substantiates the greater inhibitory potential of pyrazinone derivated compared to isoniazid (**Figures S7** and **S14**). Furthermore, dynamic cross-correlation motion (DCCM) plots show reduced anti-correlation between residues in complexes containing pyrazinone derivatives in comparison to the isoniazid: InhA complex, whereas the apoprotein exhibits the highest degree of anti-correlated motion (**Figures S15–S19** [SI, https://doi.org/10.5281/zenodo.15537581]), which points to the attained stabilization upon ligand binding. Overall, these analyses provide clues to the inhibitory potential of pyrazinone derivations toward InhA.

Arg194 is the common anchor point for all ligands within the InhA binding pocket

Pre-simulation molecular docking calculations reveal that all pyrazinone derivatives (**I–VIII, Figure 1**) interact with InhA at a congruous binding site (**Figure 4**) that

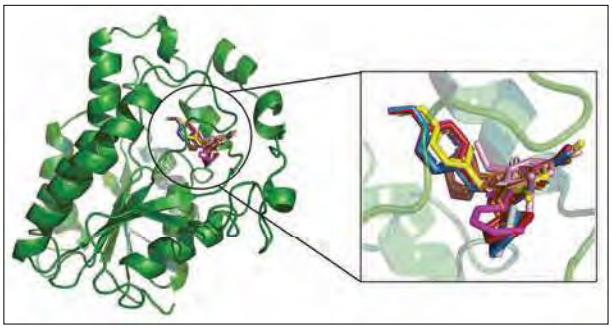

Figure 4: Superposition of all the docked structures containing ligands I–VIII bound to InhA

involves Arg194 as the common anchoring point (**Figure 5**). Further, the hydrogen-bonding interactions of Arg194 with each of these ligands are retained during simulations (45–99% occupancies, **Figure 6**) and are distinctly observed in the last simulation frame for most complexes (**Figure 7**). Furthermore, except in complex I, the interaction of Arg194 with the ligand is retained even in the optimized isolated quantum chemical models of all complexes, which points to the intrinsically stable nature of these interactions (**Figure 8**).

Although the docked structures reveal hydrogen bonding of the side chain of Arg194 with the carbonyl oxygen (complexes **I, II, III,** and **IV**) or N1 (complexes **V, VI, VII,** and **VIII**), MD simulations and QM calculations reveal the interaction of Arg194 with carboxylate and/or carbonyl oxygen atoms of the pyrazinone skeleton of each ligand (**Figures 7 and 8**). Altogether, this suggests that Arg194 plays an important role in the binding of pyrazinone derivatives. In addition to Arg194, the interaction with Ile193 is important for ligand binding. Specifically, although docking reveals that Ile193 interacts with only two ligands (**IV** and **VI**), simulations suggest significant (43.6–96.1%) occupancy of this interaction in complexes containing five (i.e., **II, III, V, VII,** and **VIII**) of the eight ligands (**Figure 6**). Further, except for the complex containing ligand **VI**, the interaction of Ile193 is retained in the last frame of the simulations of all complexes (**Figure 7**), suggesting that this residue plays an important role in active-site organization and ligand binding. This is further substantiated by QM calculations,

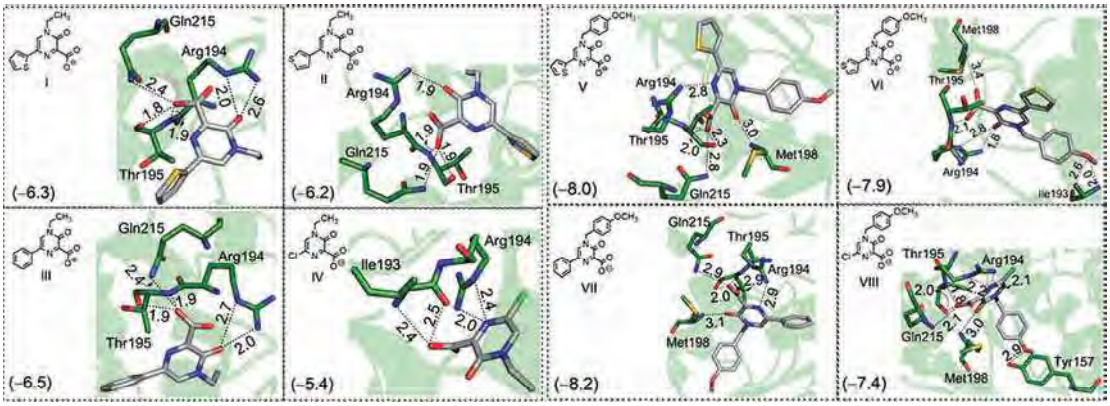

Figure 5: Hydrogen bonding interactions (dotted lines) between the carboxylate-ionized form of *N*4-ethyl (I–IV) and *N*4-methoxybenzyl (V–VIII) substituted pyrazinone derivatives and the binding-site residues of InhA in the complexes obtained from molecular docking. Hydrogen-bonding interactions were determined using a donor-acceptor cutoff distance of 3.4 Å and a donor-hydrogen-acceptor cutoff angle of 120˚. Hydrogen bonding donor-acceptor distances (Å) are provided. Docking scores (kcal/mol) are also provided in parentheses

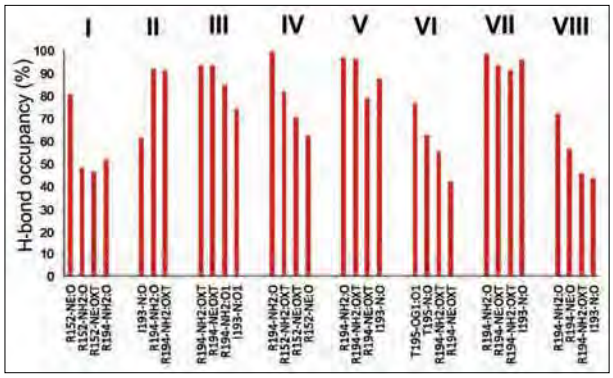

Figure 6: Percent occupancies of the important hydrogen-bonding interactions between the carboxylate-ionized forms of the ligands and the InhA residues within the simulation time. Hydrogen-bonding interactions were determined using a donor-acceptor cutoff distance of 3.4 Å and a donor-hydrogen-acceptor cutoff angle of 120˚

which reveal intrinsically stable interaction of this residue with four (i.e., **III, V, VII,** and **VIII**) ligands (**Figure 8**).

More importantly, analysis of the structures from the last simulation frame of each complex reveals that although ligand: protein interactions slightly differ between the docked and simulated structures, all pyrazinone derivatives remain intact within the binding pocket till the end of the simulation (**Figure 5** and **7**). Docking further reveals that all *N*4-ethyl ligands containing an aromatic moiety at C6 (i.e., **I, II,** and **III**) hydrogen bond with Arg194, Thr195, and Gln215, although the C6-chloro-substituted ligand (**IV**) additionally interacts with Ile193 (**Figure 5**). However, the four *N*4-methoxybenzyl substituted analogs **(V–VIII)** interact with Arg194, Thr195, and Met198, although ligands containing 2-thiophene (**V**), phenyl (**VII**) or chloro (**VIII**) substitution at C6 additionally hydrogen bond with Gln215 (**Figure 5**). Further, a salt bridge interaction is observed between the negative carboxylate group of each ligand and the positively charged guanidinium side chain of Arg194 (**Table 1**). Furthermore, MD simulations suggest that the hydrogen bonding occupancies of the

Table 1: Comparison of the residues forming hydrophobic interactions in the docked complexes of InhA and the simulated structures with ionized pyrazinone derivatives (I–VIII, Figure 1).

Ligand	Docked Complex	Simulated Complex (Last frame)
I	Thr195, Ala197	Val237
II	Thr195, Met198	Ile201, Pro155, Thr195, Val237
III	Thr195, Aal197, Met198, Ile201	Thr195, Aal197, Met198
IV	Met198	-
V	Tyr157, Met198, Ile201	Ile201, Met146, Phe96
VI	Ile201, Asp149, Arg152, Thr195	-
VII	Arg152, Tyr157, Met198, Ile201	Arg190, Ile193, Ile201
VIII	Tyr157, Met198, Ile201	Phe148, Tyr157

complexes containing *N*4-methoxybenzyl substituted ligands (maximum occupancy of 97.2% for **V**, 76.9% for **VI**, 98.5% for **VII** and 72.2% for **VIII**) are comparable to that of complexes containing N4-ethyl substituted ligands (80.7% for **I**, 91.9% for **II**, 93.6% for **III,** and 99.6% for **IV**, **Figure 6**). In comparison, isoniazid interacts at the different binding sites of InhA, and hydrogen bonds with Pro150, Met154, Pro155, and Thr161 (**Figure S22** [SI, https://doi.org/10.5281/zenodo.15537581]), although the last MD frame and QM-optimized structure show the interaction of isoniazid with Asp149, Tyr157 (**Figure S23** [SI, https://doi.org/10.5281/zenodo.15537581]), and Asp149, Arg152, Pro155 (**Figure S24** [SI, https://doi.org/10.5281/zenodo.15537581]), respectively.

The neutral (i.e., COOH) form of each ligand was also examined for comparison. Docking reveals that, like the complexes containing the carboxylate-ionized form, Arg194 is the common anchoring residue for each ligand

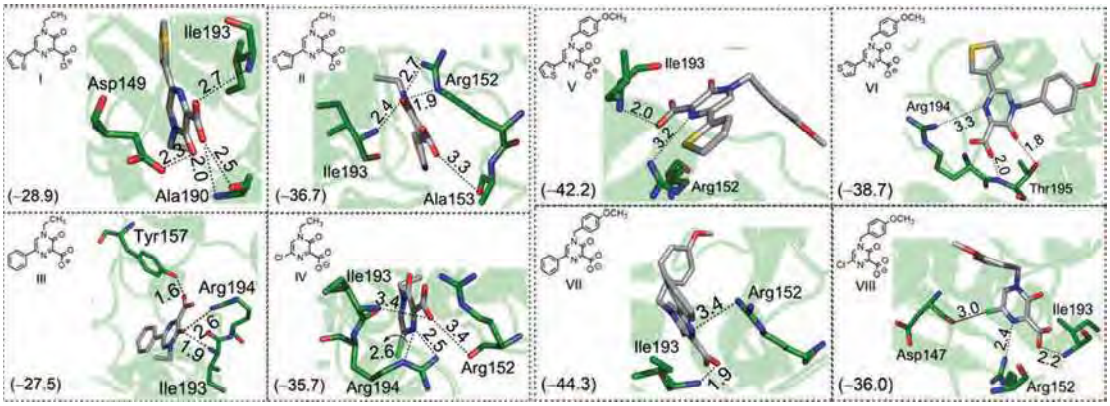

Figure 7: Hydrogen bonding (dotted lines) and halogen bonding (bold line) interactions between the carboxylate-ionized form of N4-ethyl (I–IV) and N4-methoxybenzyl (V–VIII) substituted pyrazinone derivatives and the binding-site residues of InhA in the complexes obtained from the last simulation frame. Hydrogen-bonding interactions were determined using a donor-acceptor cutoff distance of 3.4 Å and a donor-hydrogen-acceptor cutoff angle of 120°. Hydrogen bonding donor-acceptor distances (Å) are provided. MM-GBSA binding enthalpies (kcal/mol) are also provided in parentheses

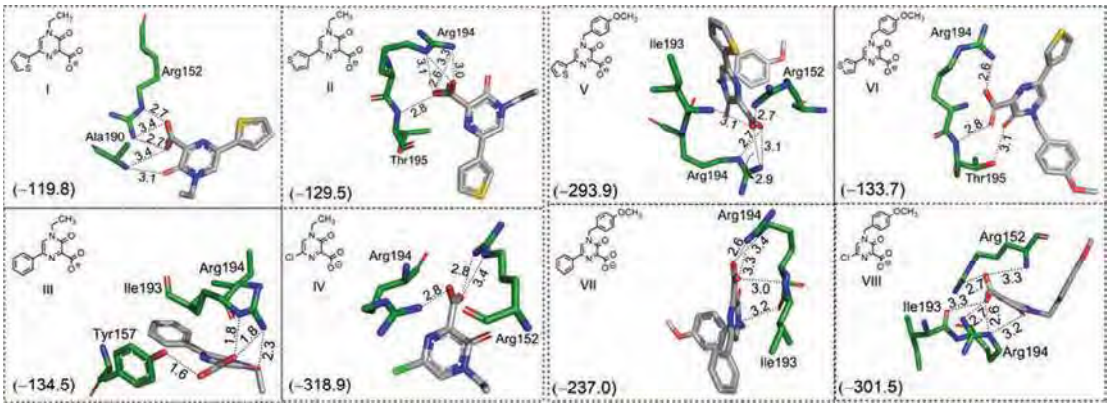

Figure 8: Quantum mechanical (QM) optimized structures of the model complexes involving the carboxylate-ionized form of N4-ethyl (I–IV) and N4-methoxybenzyl (V–VIII) substituted pyrazinone derivatives and the hydrogen bonding residues, derived from the last simulation frame. Basis set superposition error-corrected interaction energies (kcal/mol) are provided in parentheses

(**Figure S22**). Further, except **IV**, Arg194 interacts with all neutral ligands in MD simulations (80–90% occupancy, **Figure S21** [SI, https://doi.org/10.5281/zenodo.15537581]) and QM-optimized structures (**Figure S24**). Similarly, the interaction with Ile193 was also observed in simulations (**Figure S21**) and QM-optimized structures (**Figure S24**) and distinctly in the last simulation frame of most complexes (**Figure S23**). However, due to significant similarities in the interactions of neutral and ionized ligand forms and the greater importance of the ionized ligand form at physiological pH, only the complexes containing ionized ligands are discussed in the subsequent sections.

Ligands show variable hydrophobic interactions with the amino-acid residues of InhA

In addition to hydrogen bonding, the ligands form hydrophobic contacts with the receptor through their N4 and C6 moieties (**Table 1**). Molecular docking reveals that Met198 most commonly forms hydrophobic contacts with ligands (i.e., with **II, III, IV, V, VII,** and **VIII**, **Table 1**), although this interaction is retained in the last frame of simulation only by complex **III** (**Table 1**). Further, Ile 201 forms hydrophobic contacts with all the four docked N4-methoxybenzyl substituted ligands **(V–VIII)**, where Tyr157 and Arg152 form additional hydrophobic contacts with three (**V, VII,** and **VIII**) and two (**VI** and **VII**) ligands, respectively (**Table 1**). In contrast, except ligand **IV**, Thr195 interacts with N4-ethyl substituted ligands, whereas Ala197 additionally interacts with ligands **I** and **III** (**Table 1**).

However, the interaction of the ligand with Ile201 in the last frame of simulation is retained in complex **V** and **VII** only and introduced in complex **II**, whereas interaction with Thr195 is retained in complex **II** and **III,** and interaction with Tyr157 is retained in complex **VIII**. Further, new hydrophobic interactions occur in simulations (interaction with Val237 in complex **I**; Pro155, Ile201, Val237 in complex **II**; Phe46, Met146 in complex **V**; Arg190, Ile193 in complex **VII** and Phe148 in complex **VIII**), while the interactions observed in docked structures are lost (**Table 1**). However, in the case of isoniazid bound InhA, the interaction of Tyr157 with isoniazid is observed in both the docked and simulated complex, along with the interaction of Pro150 (**Table S2**). Overall, this analysis suggests that due

to their weak nature, hydrophobic interactions show variable behavior in simulations.

N4-methoxybenzyl substituted compounds show more effective binding with InhA

Docking reveals that *N*4-methoxybenzyl substituted ligands **(V–VIII)** show better receptor binding (docking scores of –7.4 to –8.2 kcal/mol) than *N*4-ethyl substituted ligands (**I–IV**, docking scores of –5.4 to –6.5 kcal/mol, **Table 2**), where all ligands show stronger binding than isoniazid (–5.4 kcal/mol, **Tables 2** and **S4** [SI, https://doi.org/10.5281/zenodo.15537581]). Stronger binding of *N*4-methoxybenzyl substituted ligands is further substantiated by post-simulation MM-GBSA binding energy values, which are significantly higher (–36.0 to –44.3 kcal/mol) compared to *N*4-ethyl substituted compounds (–27.5 to –36.7 kcal/mol, **Table 2**). On similar lines, QM calculations on reduced models reveal that the average binding strength of *N*4-methoxybenzyl substituted ligands (–241.5 kcal/mol) is higher than four *N*4-ethyl substituted compounds (–175.6 kcal/mol). Overall energy calculations (Docking score + MMGBSA binding energies + QM binding energies) summarize the enhanced stability of complexes containing *N*4-methoxybenzyl substituted ligands. Further, out of the four *N*4-methoxybenzyl substituted ligands, ligand **VII** with C6-chloro substitution shows the greatest stability (**Table 2**).

MATERIALS AND METHODS

Initial 3D structures of InhA and ligands

The X-ray crystal structure of the InhA protein of *Mtb* (PDB ID: 4U0J)[35] was used as a starting point for this study. The co-substrate, bound ligand, and water molecules were removed from the structure using PyMOL.[36] Initial 3D structures of the ligands were prepared using GaussView 6.0.[37]

Docking-based virtual screening

Molecular docking was performed using AutoDock 4.0.2.[38] Specifically, the protein and ligands were prepared using AutoDock Tools 1.5.6,[39] which converts PDB files into PDBQT format after the addition of the polar hydrogen atoms to the receptor using the 'hydrogen' module.

Table 2: Docking scores, MM-GBSA enthalpy values, and binding energies of optimized quantum-mechanical (QM) models of InhA complexes with ionized pyrazinone derivatives (I–VIII, Figure 1).

Ligand	Docking scores (kcal/mol)	MM-GBSA (kcal/mol)	QM (kcal/mol)
I	–6.3	–28.9	–119.8
II	–6.2	–36.7	–129.5
III	–6.5	–27.5	–134.5
IV	–5.4	–35.7	–318.9
V	–8.0	–42.2	–293.9
VI	–7.9	–38.7	–133.7
VII	–8.2	–44.3	–237.0
VIII	–7.4	–36.0	–301.5

Subsequently, Kollman's united atom partial charges were assigned to each receptor atom. The centroid of the region encompassing the Gly95, Met154, Tyr157, Met160, Val202, Leu217, and Glu218 receptor residues that directly interact with the ligand in the reported crystal structure,[35] was used to prepare the grid box of size 56 Å X 54 Å X 74 Å, with 0.430 Å grid spacing. Molecular docking was performed using the Lamarckian genetic algorithm,[40] with a maximum of 2,500,000 energy evaluations, an initial 150 randomly placed individuals, up to 27,000 generations, 0.02 mutation rate, 0.80 crossover rate, and elitism value (number of top individuals that automatically survive) of 1.

MD simulations

MD simulations were performed on the docked complexes, as well as the apo form of the InhA protein, using the AMBER 20 suite of programs.[41] In accordance with previous studies,[42,43] partial atomic charges for each ligand were calculated at the HF/6-31G(d) level using the RESP ESP Charge Derive (RED version 2.0) server.[44] These calculations were initiated using the stable conformation of each ligand obtained from B3LYP/6-31G(d,p) gas-phase geometry optimizations using Gaussian 09.[45] Each complex was charge neutralized using the appropriate number of Na^+, hydrated using a 10 Å box of TIP3P water molecules,[46] and simulated using the ff14SB force field.[47] Na^+ was modeled using Joung and Cheatham's ion parameters.[48]

In the first step, each hydrated complex was energy minimized using a tandem sequence of 10000 steepest descent and 10000 conjugate gradient steps, with the solute held fixed using a 500 kcal/mol Å^2 restraint. In the second step, the entire box containing the solute and solvent was energy minimized using the same number and sequence of minimization steps. The Langevin temperature equilibrium scheme[49,50] was subsequently employed, and the system was gradually heated from 0 K to 300 K in 60 K increments by carrying out small (40 ps) constant volume simulations, using the solute restraint of 10 kcal/mol Å^2. Subsequently, after carrying out a 40 ps constant-volume simulation at 300 K, the restraint was reduced to 5 kcal/mol Å^2, and the system was further simulated for 40 ps. This process was repeated using a 1.5 kcal/mol Å^2 solute restraint. Finally, a 500 ns MD simulation was carried out on each system at 1 atm and 300 K by constructing an NPT ensemble built from a Monte Carlo barostat and a Langevin thermostat.[51] This amounts to a total of 9 µs simulation data for 18 systems (eight complexes involving the carboxylic-ionized forms of ligands, eight complexes involving the unionized (neutral) ligands, one complex involving isoniazid, and one unbound (apo) form of InhA). A hydrogen mass repartition scheme[52] was applied in the heating and production steps to ensure the use of a longer (4 fs) time step.

Simulation analysis

Structural visualization was carried out using PyMOL.[36] Additional analyses were performed using the cpptraj module of AmberTools.[53] Specifically, the RAC was analyzed to determine the simulation convergence (**Figures S3** and **S4** [SI, https://doi.org/10.5281/zenodo.15537581]). Further, the RMSD of the protein backbone atoms of each system

was evaluated with respect to the first production simulation frame. Furthermore, RMSF of the Cα atoms of each InhA residue about their initial positions were calculated to compare their positions in the protein before and after ligand binding. Further, the radius of gyration (RoG) was calculated for each complex and compared with the free protein to evaluate the extent of protein folding or loosening on ligand binding and solvent-accessible surface area (SASA), which estimates the extent of active site hydration, was measured.

PCA was performed to separate large-scale macromolecular motions from random motions. This analysis groups together the molecular conformational similarities and measures the variabilities in terms of the directional eigenvalues (PC1 and PC2).[54] PC1 and PC2 of the simulated complexes were plotted to compare the flexibility patterns in the analyzed complexes. Further, DCCM analysis was performed on each simulation to analyze the magnitude of the correlation coefficient between different residues of InhA. This analysis uses the directional motion of the Cα atoms of different residues to determine the correlated motions within different macromolecular domains.[55] The values of pairwise cross-correlations range from –1 to 1, where positive values indicate that the motions of the two residues are correlated (i.e., move in the same direction), and the negative values represent the anti-correlated (i.e., opposing) motions. The occupancy of each protein: ligand hydrogen bond was calculated using the "hbond" command of cpptraj, using the donor-acceptor cutoff distance of 3.4 Å and a donor-hydrogen-acceptor cutoff angle of 120°.[42,43]

MMGBSA calculations

MMGBSA calculations were conducted using the 5000 equally spaced frames selected from the trajectory of each ligand-bound complex generated after removing water and Na^+ to estimate the binding free energies. Within these calculations, the binding free energy is calculated from the energy difference between the complex and the unbound form using a simple thermodynamic cycle.[56] These calculations were carried out using the MMGBSA.py module of Amber 20.[41]

Quantum chemical calculations

Quantum-chemical geometry optimizations were carried out to further understand the stability of the hydrogen-bonding network formed within the protein: ligand complexes. Specifically, the structure of the ligand and the interacting amino-acid residues were extracted from the last simulation frame of each complex using PyMOL[36] and Gaussview 6.0.[37] The C- and N-terminals of the interacting amino acids were truncated by adding hydrogen atoms. Geometry optimizations of these complexes were performed at the B3LYP/6-31(d,p) level. Further, the basis set superposition error corrected interaction energy of each of these models was estimated at the B3LYP/6-311+G(2df,p) level. All quantum chemical calculations were performed using Gaussian 09.[45]

CONCLUSION

In this study, we employed a structure-based approach to design and analyze potential inhibitors for the InhA receptor of *Mtb* using molecular docking, MD simulations, MMGBSA free energy measurements, and quantum mechanical calculations. Molecular docking indicates that the binding strength of pyrazinone derivatives to InhA is greater than isoniazid, the known first-line anti-TB drug. Further, the *N*4-methoxybenzyl substituted derivatives show higher docking scores than their *N*4-ethyl counterparts and thus bind more strongly with InhA. MD simulations reveal lower backbone RMSD of the complexes compared to the apo form of InhA, and point to enhanced stability of the binding pocket after inhibitor binding. Further, RoG and SASA results indicate that the inhibitors remain intact in the binding pocket of the protein and indicate the structural compactness of each complex. Similarly, PCA analysis points to the reduced protein flexibility and decreased functional capacity of the protein. RMSF analysis also suggests decreased fluctuations after ligand binding. Further, docking studies and simulations reveal that Arg194 is the common residue forming hydrogen bonding with all pyrazinone derivatives. Further, Ile193 also shows hydrogen bonding with five out of eight ligands, and other active site residues such as Thr195, Met198, Ile201, and Gln215 also show interactions with the ligands. Finally, MMGBSA enthalpy values for compounds having *N*4-methoxybenzyl substitution are higher than compounds having *N*4-ethyl substitution. Quantum mechanical calculations further substantiate these conclusions, proposing greater inhibitory potential of *N*4-methoxybenzyl substituted compounds toward InhA. Overall, the compound (**VII**) with *N*4-methoxybenzyl and C6-phenyl substitution shows maximal binding and inhibition efficiency out of all pyrazinone derivatives studied in this work. The structural and energetic studies in this work provide significant insights for designing new inhibitors against InhA for treating TB.

CONFLICTS OF INTEREST

The authors declare that they have no known competing financial interests or personal relationships that could have appeared to influence the work reported in this paper.

ACKNOWLEDGMENTS

AG and IN thank UGC for a Senior Research Fellowship. The authors gratefully acknowledge financial support for the project from the Natural Sciences and Engineering Research Council of Canada (JFT: grant # 2018-06338). All authors wish to recognize that this work was made possible by the facilities of the Shared Hierarchical Academic Research Computing Network (SHARCNET: www.sharcnet.ca) and Compute/Calcul Canada, now known as the Digital Research Alliance of Canada (https://alliancecan.ca/en).

REFERENCES

[1] Delogu, G., Sali, M. and Fadda, G. The biology of *Mycobacterium tuberculosis* infection, *Mediterr. J. Hematol. Infect. Dis.*, **2013**, *5*, e2013070.

[2] Rajasekhar, S., Karuppasamy, R. and Chanda, K. Exploration of potential inhibitors for tuberculosis via structure-based drug design, molecular docking, and molecular dynamics simulation studies, *J. Comput. Chem.*, **2021**, *42*, 1736–1749.

[3] Chakaya, J., Petersen, E., Nantanda, R., Mungai, B.N., Migliori, G.B., Amanullah, F., Lungu, P., Ntoumi, F., Kumarasamy, N., Maeurer, M. and Zumla, A. The WHO Global tuberculosis 2021 report-not so good news and turning the tide back to end TB, *Int. J. Infect. Dis.*, **2022**, *124*, S26–S29.

[4] Glaziou, P. *Predicted Impact of the COVID-19 Pandemic on Global Tuberculosis Deaths in 2020*, [MedRxiv Preprint], **2020**.

[5] Espinal, M.A. The global situation of MDR-TB, *Tuberculosis* (*Edinb*), **2003**, *83*, 44–51.

[6] Denholm, J.T., McBryde, E.S., Eisen, D.P., Penington, J.S., Chen, C. and Street, A.C. Adverse effects of isoniazid preventative therapy for latent tuberculosis infection: A prospective cohort study, *Drug Healthc. Patient Saf.,* **2014**, *6*, 145–149.

[7] World Health Organization. *Global Tuberculosis Report 2020*, WHO, Geneva, Switzerland, **2020**.

[8] Gygli, S.M., Borrell, S., Trauner, A. and Gagneux, S. Antimicrobial resistance in Mycobacterium tuberculosis: Mechanistic and evolutionary perspectives, *FEMS Microbiol. Rev.,* **2017**, *41*, 354–373.

[9] Jarlier, V. and Nikaido, H. Mycobacterial cell wall: Structure and role in natural resistance to antibiotics, *FEMS Microbiol. Lett.*, **1994**, *123*, 11–18.

[10] Daffe, M. and Draper, P. The envelope layers of mycobacteria with reference to their pathogenicity, *Adv. Microb. Physiol.*, **1997**, *39*, 131–203.

[11] Barry, C.E 3rd., Lee, R.E., Mdluli, K., Sampson, A.E., Schroeder, B.G., Slayden, R.A. and Yuan, Y. Mycolic acids: Structure, biosynthesis and physiological functions, *Prog. Lipid Res.*, **1998**, *37*, 143–179.

[12] Pawełczyk, J. and Kremer, L. The molecular genetics of mycolic acid biosynthesis, *Microbiol. Spectr.*, **2014**, *2*, 611-631.

[13] Marrakchi, H., Lanéelle, M.A. and Daffé, M. Mycolic acids: Structures, biosynthesis, and beyond, *Chem. Biol.*, **2014**, *21*, 67–85.

[14] Schroeder, E.K., De Souza, O.N., Santos, D.S., Blanchard, J.S. and Basso, L.A. Drugs that inhibit mycolic acid biosynthesis in *Mycobacterium tuberculosis*, *Curr. Pharm. Biotechnol.*, **2002**, *3*, 197–225.

[15] Kouassi, A.F., Kone, M., Keita, M., Esmel, A., Megnassan, E., N'Guessan, Y.T., Frecer, V. and Miertus, S. Computer-aided design of orally bioavailable pyrrolidine carboxamide inhibitors of enoyl-acyl carrier protein reductase of *Mycobacterium tuberculosis* with favorable pharmacokinetic profiles, *Int. J. Mol. Sci.*, **2015**, *16*, 29744–29771.

[16] Vilchèze, C., Morbidoni, H.R., Weisbrod, T.R., Iwamoto, H., Kuo, M., Sacchettini, J.C. and Jacobs, W.R. Jr. Inactivation of the inhA-encoded fatty acid synthase II (FASII) enoyl-acyl carrier protein reductase induces accumulation of the FASI end products and cell lysis of *Mycobacterium smegmatis*, *J. Bacteriol.*, **2000**, *182*, 4059–4067.

[17] Vilchèze, C. Mycobacterial cell wall: A source of successful targets for old and new drugs, *Appl. Sci.,* **2020**, *10*, 2278.

[18] Slayden, R.A. and Barry, C.E 3rd. The genetics and biochemistry of isoniazid resistance in *Mycobacterium tuberculosis*, *Microbes Infect.*, **2000**, *2*, 659–669.

[19] Slayden, R.A., Lee, R.E. and Barry, C.E 3rd. Isoniazid affects multiple components of the type II fatty acid synthase system of *Mycobacterium tuberculosis*, *Mol. Microbiol.*, **2000**, *38*, 514–525.

[20] Rajalakshmi, G., Pavan, M.S. and Kumaradhas, P. Charge density distribution and electrostatic interactions of ethionamide: An inhibitor of the enoyl acyl carrier protein reductase (inhA) enzyme of *Mycobacterium tuberculosis*, *RSC Adv.*, **2014**, *4*, 57823–57833.

[21] Vilchèze, C., Wang, F., Arai, M., Hazbón, M.H., Colangeli, R., Kremer, L., Weisbrod, T.R., Alland, D., Sacchettini, J.C. and Jacobs, W.R. Jr. Transfer of a point mutation in *Mycobacterium tuberculosis* inhA resolves the target of isoniazid, *Nat. Med.*, **2006**, *12*, 1027–1029.

[22] Salfinger, M., Crowle, A.J. and Reller, L.B. Pyrazinamide and pyrazinoic acid activity against tubercle bacilli in cultured human macrophages and in the bactec system, *J. Infect. Dis.*, **1990**, *162*, 201–207.

[23] Yang, J., Liu, Y., Bi, J., Cai, Q., Liao, X., Li, W., Guo, C., Zhang, Q., Lin, T., Zhao, Y., Wang, H., Liu, J., Zhang, X. and Lin, D. Structural basis for targeting the ribosomal protein S1 of *Mycobacterium tuberculosis* by pyrazinamide, *Mol. Microbiol.,* **2015**, *95*, 791–803.

[24] Bishi, L.Y., Vedithi S.C., Blundell, T.L. and Mugumbate, G.C. Computational deorphaning of *Mycobacterium tuberculosis* targets. In: *Drug Discovery and Development-New Advances*, Bod - Books on Demand, Germany, **2019**.

[25] Njire, M., Tan, Y., Mugweru, J., Wang, C., Guo, J., Yew, W., Tan, S. and Zhang, T. Pyrazinamide resistance in *Mycobacterium tuberculosis*: Review and update, *Adv. Med. Sci.*, **2016**, *61*, 63–71.

[26] Tan, Y., Hu, Z., Zhang, T., Cai, X., Kuang, H., Liu, Y., Chen, J., Yang, F., Zhang, K., Tan, S. and Zhao, Y. Role of pncA and rpsA gene sequencing in detection of pyrazinamide resistance in *Mycobacterium tuberculosis* isolates from Southern China, *J. Clin. Microbiol.*, **2014**, *52*, 291–297.

[27] Haratiasl, A.A., Hamzelou, G., Amini, S., Kardan-Yamchi, J., Haeili, M., Heidari, F. and Feizabadi, M.M. Molecular identification of mutations conferring resistance to rifampin, isoniazid and pyrazinamide among *Mycobacterium tuberculosis* isolates from Iran, *J. Chemother.*, **2020**, *32*, 75–82.

[28] Dolezal, M. and Zitko, J. Pyrazine derivatives: A patent review [June 2012-Present], *Expert Opin. Ther. Pat.*, **2015**, *25*, 33–47.

[29] Kaval, N., Appukkuttan, P. and Van der Eycken, E. The chemistry of 2-(1H)-pyrazinones in solution and on solid support, in microwave-assisted synthesis of heterocycles. In: *Topics in Heterocyclic Chemistry*, Vol. 1. Springer, Berlin, Heidelberg, **2006**, p267–304.

[30] Kravchenko, M.A., Verbitskiy, E., Skornyakov, S.N., Slepukhin, P.A., Rusinov, G.L., Chupakhin, O.N. and Charushin, V.N. Synthesis and antitubercular evaluation on novel 1-ethyl-5-(hetero)aryl-1,6-dihydropyrazine-2,3-dicarbonitriles and 3-cyano-1-ethyl-5-(hetero)aryl-2(1H)-pyrazinones, *Anti Infect. Agents*, **2016**, *14*, 139–144.

[31] Mishra, R., Jha, K.K., Kumar, S. and Tomer, I. Synthesis, properties and biological activity of thiophene: A review, *Pharma Chem.*, **2011**, *3*, 38–54.

[32] Patel, A.A. and Mehta, A.G. Synthesis of novel heterocyclic compounds and their biological evaluation, *Pharma Chem.*, **2010**, *2*, 215–223.

[33] Kisten, K., Kumalo, H.M., Machaba, K.E., Ndagi, U. and Mhlongo, N.N. Drug repurposing approach against *Mycobacterium tuberculosis* Enoyl-[acyl-carrier-protein] reductase: Insight from molecular dynamics simulations, *Mol. Sim.*, **2021**, *47*, 1313–1325.

[34] Pitaloka, D.A.E., Ramadhan, D.S.F., Arfan, A., Chaidir, L. and Fakih, T.M. Docking-based virtual screening and molecular dynamics simulations of quercetin analogs as enoyl-acyl carrier protein reductase (Inha) inhibitors of *Mycobacterium tuberculosis*, *Sci. Pharm.*, **2021**, *89*, 20.

[35] He, X., Alian, A., Stroud, R. and De Montellano, P.R. Pyrrolidine carboxamides as a novel class of inhibitors of enoyl acyl carrier protein reductase from *Mycobacterium tuberculosis*, *J. Med. Chem.*, **2006**, *49*, 6308–6323.

[36] Schrodinger, L. *The PyMOL Molecular Graphics System. Version 1.3r1*, Vol. 1. Schrödinger, LLC, United States, **2010**.

[37] Dennington, R., Keith, T.A. and Millam, J.M. *GaussView 6.0. 16*, Semichem Inc., Shawnee Mission, KS, USA, **2016**.

[38] Huey, R., Morris, G.M., Olson, A.J. and Goodsell, D.S. A semiempirical free energy force field with charge-based desolvation, *J. Comput. Chem.*, **2007**, *28*, 1145–1152.

[39] Morris, G.M., Huey, R., Lindstrom, W., Sanner, M.F., Belew, R.K., Goodsell, D.S. and Olson, A.J. AutoDock4 and AutoDockTools4: Automated docking with selective receptor flexibility, *J. Comput. Chem.*, **2009**, *30*, 2785–2791.

[40] Morris, G.M., Goodsell, D.S., Halliday, R.S., Huey, R., Hart, W.E., Belew, R.K. and Olson, A.J. Automated docking using a Lamarckian genetic algorithm and an empirical binding free energy function, *J. Comput. Chem.*, **1998**, *19*, 1639–1662.

[41] Case, D., Walker, R.C., Cheatham, T.E 3rd, Simmerling, C., Roitberg, A., Merz, K.M., Li, P.,… & Kollman, P.A. *AMBER 20*, University of California, San Francisco, **2020**.

[42] Negi, I., Kathuria, P., Sharma, P. and Wetmore, S.D. How do hydrophobic nucleobases differ from natural DNA nucleobases? Comparison of structural features and duplex properties from QM calculations and MD simulations, *Phys. Chem. Chem. Phys.*, **2017**, *19*, 16365–16374.

[43] Negi, I., Mahmi, A.S., Seelam Prabhakar, P. and Sharma, P. Molecular dynamics simulations of the aptamer domain of guanidinium ion binding riboswitch ykkC-III: Structural Insights into the discrimination of cognate and alternate ligands, *J. Chem. Inf. Model.*, **2021**, *61*, 5243–5255.

[44] Dupradeau, F.Y., Pigache, A., Zaffran, T., Savineau, C., Lelong, R., Grivel, N., Lelong, D., Rosanski, W. and Cieplak, P. The REd. Tools: Advances in RESP and ESP charge derivation and force field library building, *Phys. Chem. Chem. Phys.*, **2010**, *12*, 7821–7839.

[45] Frisch, M.J.E.A., *Gaussian 09*, *Revision A. 01*, Gaussian Inc., Wallingford, **2009**.

[46] Jorgensen, W.L., Chandrasekhar, J., Madura, J.D., Impey, R.W. and Klein, M.L. Comparison of simple potential functions for simulating liquid water, *J. Chem. Phys.*, **1983**, *79*, 926–935.

[47] Maier, J.A., Martinez, C., Kasavajhala, K., Wickstrom, L., Hauser, K.E. and Simmerling, C. ff14SB: Improving the accuracy of protein side chain and backbone parameters from ff99SB, *J. Chem. Theory Comput.*, **2015**, *11*, 3696–3713.

[48] Joung, I.S. and Cheatham, T.E 3rd. Determination of alkali and halide monovalent ion parameters for use in explicitly solvated biomolecular simulations, *J. Phys. Chem. B.*, **2008**, *112*, 9020–9041.

[49] Singer, K. and Smith, W. Path integral simulations of condensed phase Lennard-Jones systems, *Mol. Phys.*, **1988**, *64*, 1215–1231.

[50] Gillan, M. Quantum simulation of hydrogen in metals, *Phys. Rev. Lett.*, **1987**, *58*, 563.

[51] Allen, M.P. and Tildesley, D.J. *Computer Simulation of Liquids*, Oxford University Press, Oxford, **2017**.

[52] Hopkins, C.W., Le Grand, S., Walker, R.C. and Roitberg, A.E. Long-time-step molecular dynamics through hydrogen mass repartitioning, *J. Chem. Theory Comput.*, **2015**, *11*, 1864–1874.

[53] Case, D.A., Darden, T.A., Cheatham III, T.E., Simmerling, C., Wang, J., Duke, R., Luo, R., Walker, R.C., Zhang, W., Merz, K.M. and Roberts, B. *AmberTools 16*, University of California, San Francisco, **2016**.

[54] Granato, D., Santos, J.S., Escher, G.B., Ferreira, B.L. and Maggio, R.M. Use of principal component analysis (PCA) and hierarchical cluster analysis (HCA) for multivariate association between bioactive compounds and functional properties in foods: A critical perspective, *Trends Food Sci. Technol*., **2018**, *72*, 83–90.

[55] Gschwend, D.A., Good, A.C. and Kuntz, I.D. Molecular docking towards drug discovery, *J. Mol. Recognit.*, **1996**, *9*, 175–186.

[56] Zhu, T., Lee, H., Lei, H., Jones, C., Patel, K., Johnson, M.E. and Hevener, K.E. Fragment-based drug discovery using a multidomain, parallel MD-MM/PBSA screening protocol, *J. Chem. Inf. Model.*, **2013**, *53*, 560–572.

Received: 28 Apr 2025; Accepted: 10 Jun 2025

Indian Journal of Heterocyclic Chemistry
Vol. 35 - Number 01 (Jan-Mar 2025) 19-24
https://connectjournals.com/01951.2025.35.19
https://doi.org/10.59467/IJHC.2025.35.19

ISSN (Print) : 0971-1627
ISSN (Online) : 2456-4311

Artabscoumarin, an unusual coumarin derivative from *Artemisia absinthium* with cytotoxic activity on cancer cells

Samy K. El-Desouky

Department of Physical Sciences-Chemistry Division, College of Science, Jazan University, P.O. Box 114, Jazan 45142, Kingdom of Saudi Arabia

ABSTRACT Investigation of the chemical constituents in the aerial parts of *Artemisia absinthium* led to the isolation and identification of one unique coumarin featuring a rare 2-hydroxypropanoic acid side chain, named artabscoumarin (**1**), as well as four phenolic compounds identified as casticin (**2**), artemetin (**3**), 7-methoxy-isobiflorin (**4**), and diosmetin-7-*O*-β-D-glucopyranoside (**5**). Their structures were elucidated using extensive spectroscopic analysis and by comparison with data reported in the literature. Compound **4** was isolated from this plant for the 1st time. In the preliminary assays, artabscoumarin (**1**) was tested by MTT colorimetric assay method for cytotoxicity against breast cancer cell lines (MCF-7), colon cancer cell lines (HT-29), and hepatocellular carcinoma cell lines (HepG2). It exhibits moderate cytotoxic activity with IC_{50} values of 29.0, 28.6, and 54.4 µg/mL, respectively.

KEYWORDS *Artemisia absinthium*, Phenolics, Coumarins, Cytotoxic activity, NMR

How to cite this article: El-Desouky, S.K. Artabscoumarin, an unusual coumarin derivative from *Artemisia absinthium* with cytotoxic activity on cancer cells, *Indian J. Heterocycl. Chem.*, **2025**, *35*, 19–24. *https://doi.org/10.59467/IJHC.2025.35.19*

INTRODUCTION

Artemisia is one of the largest genera of the family *Asteraceae*. It comprises more than 400 species distributed in South Africa, Asia, North America, and Europe. Plants of the genus *Artemisia* are represented in Saudi Arabia by seven species, namely *Artemisia absinthium*, *Artemisia monosperma*, *Artemisia sieberi*, *Artemisia scoparia*, *Artemisia judaica*, *Artemisia herba-alba*, *and Artemisia abyssinica*, most of them have been found to be used in folk medicine.[1]

A. absinthium L., commonly known as wormwood, is widely distributed in the Mediterranean region and Gulf countries.[2] It is a yellow-flowering medicinal bitter plant frequently used in traditional medicine as an antiparasitic and antimicrobial agent since ancient times. The analysis of aerial parts of this species has been shown to contain polyphenolic compounds, flavonoids, tannins, coumarins, carotenoids, sterols, terpenoids, and glycosides.[3-7] Extracts and essential oils of *A. absinthium* have been reported to exhibit various biological properties, including antimalarial,[8] antispasmodic,[9] antipyretic,[10] antitrypanosomal,[11] antibacterial,[12] acaricidal,[13] antioxidant,[14] and anti-inflammatory.[15]

In the process of our continuous search for bioactive phytochemicals from the medicinal plants grown in the Jazan region of Saudi Arabia, we report herein the isolation and structural elucidation of one new coumarin derivative named artabscoumarin (**1**), three known flavonoids and one chromone-C-glucoside from the aerial parts of *A. absinthium*. In addition, the study also provides data on the cytotoxic activity of artabscoumarin (**1**).

RESULTS AND DISCUSSION

Chemistry (Isolation and Characterization)

The methanol extract of the aerial parts of *A. absinthium* was fractionated and separated by chromatographic techniques. An uncommon coumarin derivative was isolated from the investigated EtOAc fraction representing a new

*Corresponding author: E-mail: sdesoky@jazanu.edu.sa

Published & Hosted by :
Journal Homepage :
www.connectjournals.com/ijhc
www.connectjournals.com

type of 8-alkoxy-substituted coumarin skeleton named artabscoumarin (**1**), together with four known phenolics, casticin (**2**), artemetin (**3**) 7-methoxy-isobiflorin (**4**), and diosmetin-7-*O*-β-D-glucopyranoside (**5**) [**Figure 1**]. The structure of artabscoumarin (**1**) was elucidated using UV, IR, HR-ESI-MS, 1D, and 2D NMR techniques. Compounds **2–5** were identified by comparing their NMR and MS spectral data [**Table 1**] with those reported in the literature.[16-22]

Several structurally distinct 7,8-dioxygenated and 5,7,8-trioxygenated coumarin derivatives have been identified from *Artemisia* species, but to our knowledge, this is the first report on the occurrence of artabscoumarin (**1**) from natural sources.

Compound **1** was obtained as a yellow amorphous solid, $[\alpha]^{25}_{D}$ +57° (*c* 0.1, CH_3OH). Its molecular formula was assigned as $C_{13}H_{12}O_6$, suggesting 8° of unsaturation, based on a pseudomolecular ion peak $[M+H]^+$ at *m/z* 265.0708 (calcd. for $C_{13}H_{13}O_6$, 265.0706) in the HR-ESI-MS (positive-ion mode). The ESI-MS (positive-ion mode) showed a pseudomolecular ion peak at *m/z* 287 $[M+Na]^+$ and a fragment ion at *m/z* 177 attributable to the loss of 2-hydroxypropanoic acid (lactic acid) moiety $[M+H-C_3H_5O_3]^+$. The UV-Vis spectrum of **1** showed absorption maxima at λ_{max} 322, 261, 237sh, and 208 nm indicating a 7,8-dioxygenated coumarin[23] whereas IR spectroscopic data of **1** displayed characteristic bands for hydroxyl (3431 cm^{-1}), carbonyl (1732 and 1712 cm^{-1}), and an aromatic ring (1637, 1568, 1452, 1178 cm^{-1}) functionalities. Extensive use of NMR techniques, including DEPT, HMQC, and HMBC, supported the unambiguous assignments of all ^1H and ^{13}C shift values in **1** [**Table 2**, supplementary data].

The most interesting feature of artabscoumarin (**1**) is the presence of the 2-hydroxypropanoic acid unit not described previously for naturally occurring coumarins. The structure of this side chain was established unambiguously by NMR data. This substituent in the form of an alkyl ether group is characterized by the presence of one methyl group at δ_H/δ_C 1.52 (3H, *d*, *J* = 7.2 Hz)/19.2, one methine group at δ_H/δ_C

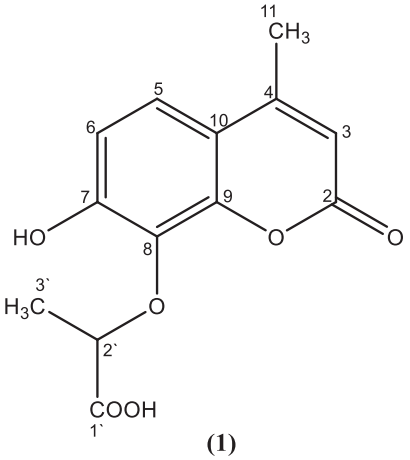

(1)

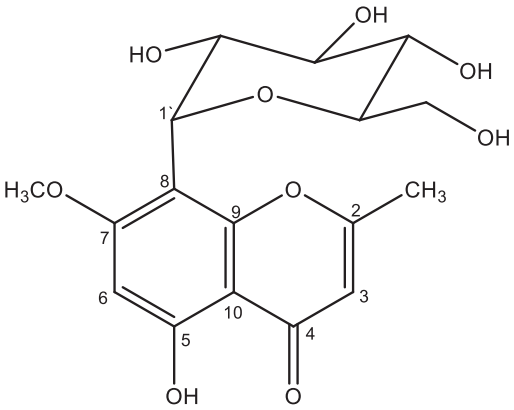

(4)

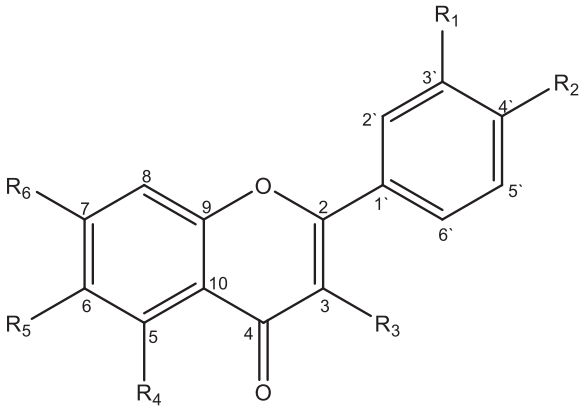

	R_1	R_2	R_3	R_4	R_5	R_6
(2)	OH	OCH_3	OCH_3	OH	OCH_3	OCH_3
(3)	OCH_3	OCH_3	OCH_3	OH	OCH_3	OCH_3
(5)	OH	OCH_3	H	OH	H	O-β-D-glucopyranoside

Figure 1: Chemical structures of compounds 1-5

Table 1: NMR spectral data of compounds 2-5 (Compounds 2,3 and 5: ^{1}H, 600 MHz, ^{13}C, 150 MHz, DMSO-d_6, δ in ppm, J in Hz and compound 4: ^{1}H, 400 MHz, ^{13}C, 100 MHz, CD_3OD, δ in ppm, J in Hz)

Position	Casticin (2)		Artemetin (3)		7-methoxy-isobiflorin (4)		Diosmetin-7-O-glucoside (5)	
	δ_H	δ_C	δ_H	δ_C	δ_H	δ_C	δ_H	δ_C
2	----	152.28	----	152.38	----	167.72	----	164.83
3	----	138.54	----	138.17	6.16, s	108.84	6.80, s	104.49
4	----	178.75	----	178.90	----	182.32	----	182.52
5	----	152.11	----	152.33	----	156.90	----	161.84
6	----	132.11	----	132.11	6.25, s	93.62	6.18 (d, J=1.8 Hz)	99.86
7	----	159.19	----	158.78	----	160.85		164.03
8	6.93, s	91.98	6.52, s	90.34	----	103.32	6.52 (d, J=1.8 Hz)	94.95
9	----	155.95	----	155.89	----	163.34	----	158.06
10	----	106.11	----	106.60	----	107.75	----	104.60
1'	----	122.54	----	122.92	----	----	----	124.80
2'	7.66 (d, J=2.3 Hz)	112.04	7.28 (d, J=2.3 Hz)	111.29	----	----	7.50 (d, J=2.2 Hz)	116.42
3'	----	148.95	----	148.80	----	----	----	150.02
4'	----	151.81	----	151.41	----	----	----	150.70
5'	7.17 (d, J=8.4 Hz)	111.20	7.01 (d, J=8.4 Hz)	110.86	----	----	7.21 (d, J=8.4 Hz)	110.80
6'	7.74 (d, J=8.4 Hz)	122.54	7.74 (d, J=8.4 Hz)	122.16	----	----	7.58 (dd, J=8.4, 2.2 Hz)	121.20
1" β-D-Glc.	----	----	----		4.65 (d, J=8.0 Hz)	73.18	5.01 (d, J=7.3 Hz)	100.03
2" β- D-Glc.	----	----	----		4.57, m	71.13	3.10–4.06*	73.61
3" β- D-Glc.	----	----	----		3.71, m	79.09	3.10–4.06*	77.15
4" β- D-Glc.	----	----	----		3.43, br	70.76	3.10–4.06*	70.16
5" β- D-Glc.	----	----	----		3.20, m	81.45	3.10–4.06*	77.34
6" β- D-Glc.	----	----	----		3.92, br and 4.03, m	61.64	3.10–4.06*	61.20
3-OCH_3	3.86, s	60.24	3.88–3.94*	60.20	----		----	----
6-OCH_3	3.93, s	60.53	3.88–3.94*	60.89	----		----	----
7-OCH_3	3.82, s	56.99	3.88–3.94*	56.34	3.56, s	56.28	----	----
3'-OCH_3	----	----		56.10	----		----	----
4'-OCH_3	3.74, s	56.14	3.88–3.94*	56.01	----		3.84 (s)	56.94
2-CH_3	----	----	----	----	2.40, s	20.34	----	----

*overlapped signals

Table 2: NMR spectral data of compound 1 (^{1}H, 600 MHz, ^{13}C, 150 MHz, DMSO-d_6, δ in ppm, J in Hz)

Position	δ_H	δ_C	HMBC (H→C)
2	-	160.04	-
3	6.09 (1H, s)	109.45	C-2, C-10, C11
4	-	153.97	-
5	7.30 (1H, d, *J*=8.4)	120.66	C-4, C-9, C-8, C-10
6	6.76 (1H, d, *J*=8.4)	113.73	C-8, C-10
7	-	156.42	
8	-	133.97	
9	-	148.06	-
10	-	111.81	-
11	2.34 (3H, s)	18.24	C-3, C-4
1'		175.61	-
2'	4.18 (1H, q, *J*=7.2)	80.59	C-8, C-1', C-3'
3'	1.52 (3H, d, *J*=7.2)	19.21	C-1', C-2'

4.18 (1H, *q*, *J* = 7.2 Hz)/80.6, and one carbonyl carbon at δ_C 175.6 in the in ^{1}H and ^{13}C NMR spectra of **1**. The NMR spectral data, combined with the IR and ESIMS data, allowed us to deduce the presence of the 2-hydroxypropanoic acid moiety. The carbon resonance at δ_C 175.6 (C-1'), together with an absorption band at 1712 cm^{-1} in the IR spectrum of **1**, indicated the presence of a free carboxylic acid group in the side chain. Moreover, the downfield shift of the methine carbon at δ_C 80.6 suggested the alkylation of this carbon instead of the esterification of the carboxylic group of the side chain.

The NMR data of the parent coumarin in **1** resembled closely to those of Rudicoumarin B, a 3,7,8-trisubstituted coumarin previously identified from *Rhadinothamnus rudis* ssp. *Amblycarpus*.[24] There are no significant differences between the NMR spectral data of the two compounds except the chemical shifts of both C-3 and C-4 which most likely arise due to the different substitution patterns on both carbons.

The ^{1}H NMR spectrum of **1** revealed two mutual *ortho*-coupling signals at δ_H 7.30 (1H, *d*, *J* = 8.4 Hz) and δ_H 6.76 (1H, *d*, *J* = 8.4 Hz), assigned to H-5 and H-6, respectively. These values are typical of a 7,8-oxygenated coumarin nucleus.[25,26] Moreover, the ^{1}H NMR spectrum showed signals at δ_H 2.34 (3H, *s*) and δ_H 1.52 (3H, *d*, *J* = 7.2 Hz) assignable to methyl groups Me-11 and Me-3', respectively. Finally, the spectrum displayed one proton signal at δ_H 6.09 (1H, *s*) assigned to H-3.

Lacking of the typical doublets for the H-3/H-4 AB system between 5.7 and 8.2 ppm of coumarins indicated a substitution at one of these two positions[25-30] and based on the aromatic protons being doublets only a 3,6,7- or 4,6,7-substitution pattern was possible for **1**. Moreover, the ^{1}H and ^{13}C NMR chemical shift values at positions C-2, C-3, and C-4 are highly similar to those of Incrassamarin D, a new 4-substituted coumarin isolated from *Calophyllum incrassatum*.[31] These findings, together with the HMBC correlations of the methyl signal at δ_H 2.34 and both of C-3 at δ_C and C-4 at δ_C 153.9, strongly suggested that the methyl group was attached to the 4-position.

The ^{13}C NMR spectrum of **1**, including DEPT and HSQC, displayed 13 carbon signals attributable to two methyl, four methine, and seven quaternary carbons. The observed upfield shift of C-3 and downfield shifts of C-4 and C-8 with respect to the corresponding unsubstituted carbons confirmed the presence of C-4 methyl group and C-8 lactic acid moiety. Moreover, the downfield nature of the chemical shift of C-7 indicated the presence of a free hydroxyl group at this position. The connection among the substituents and the parent coumarin was confirmed by analyzing some key long-range ^{1}H-^{13}C correlations in the HMBC spectrum.

In the HMBC spectrum of **1** [**Figure 2**], the position of the methyl group was confirmed from HMBC correlations of Me-11 (δ_H 2.34) with C-3 (109.4) and C-4 (153.9), whereas H-3 (δ_H 6.09)) showed long-range correlations with C-2 (160.0), C-10 (111.8), and C-11 (18.2). In addition, HMBC correlations of the methine proton (δ_H 4.18) and both C-8 (133.9) and C-3' (19.2) confirmed a linkage between the 2-hydroxypropanoic acid moiety and C-8 of the coumarin.

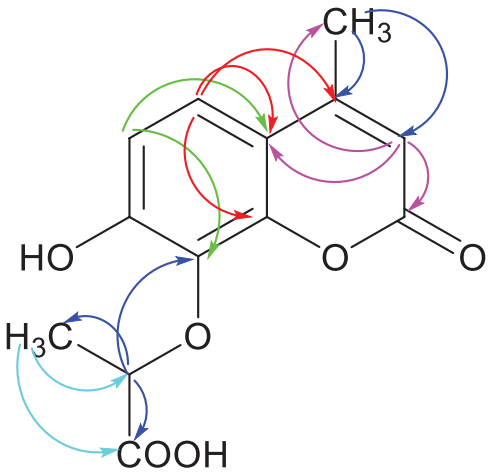

Figure 2: Key HMBC correlations of compound 1

The absolute configuration of C-2' was not resolved in this study and remains to be determined because suitable single crystals for X-ray analysis were not available. Thus, the structure of **1** was assigned as shown and named artabscoumarin.

Cytotoxicity bioassay

Compound **1** was evaluated for its cytotoxicity against three human cancer cell lines, including breast cancer cell lines (MCF-7), colon cancer cell lines (HT-29), and hepatocellular carcinoma cell lines (HepG2) by MTT colorimetric assay method[32] and showed moderate cytotoxic effect with IC_{50} values of 29.0, 28.6, and 54.4 µg/mL, respectively.

EXPERIMENTAL

General experimental procedures

UV spectra were recorded on an HP Aglient 8453 (Agilent Technologies, Santa Clara, CA, USA). Optical rotations were recorded on a Perkin-Elmer 241MC automatic polarimeter. Infra-Red spectra were obtained on a Bruker IFS spectrometer (Bruker, Billerica, MA, USA). ESI-MS was performed on the Finnigan MAT SSQ 7000 instrument (Finnigan MAT, San Jose, CA, USA). NMR spectra were obtained on Bruker AM-600 Spectrometer (Bruker, Zurich, Switzerland) with TMS as the internal standard. Deuterated solvents for NMR (DMSO and CD_3OD) were purchased from Cambridge Isotope Laboratory (Tewksbury, MA, USA). Sephadex LH-20 (Lipophilic Sephadex, 25–100 µm, Sigma-Aldrich, USA) and Polyamide 6S (50–160 µm, Fluka Chemie AG, Switzerland) were used for column chromatography. Silica gel 60 F254 plates (E. Merck, Darmstadt, Germany) were used for thin-layer chromatography. The chromatograms were visualized under UV light and then sprayed with anisaldehyde and ethanolic solution of aluminum chloride. Whatman filter paper 1MM and 3MM (Whatmann Ltd., Maidstone, Kent, England) was used for paper chromatography. Analytical-grade reagents and solvents were purchased from Sigma-Aldrich (St. Louis, MO, USA).

Plant material

The fresh aerial parts of *A. absinthium* L. were collected from Wadi Lejib road and Jabal Fayfa in Jazan region, Saudi Arabia in March 2023 during the flowering stage of the plant and identified by a plant taxonomist at the Department of Botany, College of Science, Jazan University. A voucher specimen JU/COP/23-6 has been deposited in Jazan University Herbarium (JAZUH).

Extraction and isolation

The dried aerial parts of *A. absinthium* (850 g) were extracted thrice with methanol (MeOH) (3 × 2 L) at room temperature (24 h each). The combined extract was filtered and evaporated using a rotary vacuum evaporator (Buchi, Switzerland) under low pressure at 45°C to obtain a sticky dark gum (62.4 g). The crude extract was suspended in

500 ml water and successively partitioned with *n*-hexane, dichloromethane (CH_2Cl_2), ethyl acetate (EtOAc), and *n*-butanol (BuOH). Each fraction was concentrated *in vacuo* and stored in the refrigerator at 4°C until required study.

The combined EtOAc fraction (3.2 g) was loaded to a silica gel column eluted with a gradient system of CH_2Cl_2:MeOH with increasing polarity to obtain four main fractions (F1–F4). Fraction F1 was re-chromatographed using a silica gel column eluted with isocratic system CH_2Cl_2:MeOH (3:1) to give compound **3 (**85 mg) as a yellowish amorphous powder. Fraction F2 was subjected to a silica gel column using CH_2Cl_2:MeOH (1:1) to afford a yellowish amorphous powder of compound **2 (**56 mg). Fraction F3 was subjected to repeated preparative paper chromatography using BAW (*n*-butanol: acetic acid: water, 4:1:5, upper layer) and 15% acetic acid to afford compounds **4 (**130 mg) and **5 (**16 mg) which were further purified over a Sephadex LH-20 column chromatography with EtOH: MeOH (1:1). Fraction F4 was chromatographed on a silica gel column eluted with EtOAc: MeOH (2:1) to give yellow amorphous solid of compound **1 (**46 mg).

Artabscoumarin (1)

Yellow amorphous solid. $[\alpha]^{25}_{D}$ +57° (*c* 0.1, CH_3OH); IR (KBr) ν_{max} $cm^{-1:}$ 3431, 2968, 2855, 1732, 1712, 1637, 1568, 1452, 1324, 1178, 1031, 748; UV (CH_3OH) λ_{max} nm (log ε): 322 (3.67), 261 (2.84), 237 sh (2.98), 208 (3.31); HR-ESI-MS: *m/z* 265.0708 $[M+H]^+$ (calcd. for $C_{13}H_{13}O_6$, 265.0706); ^{1}H NMR (DMSO-d_6, 600 MHz) and ^{13}C NMR (DMSO-d_6, 150 MHz).

Cytotoxicity bioassay

The cytotoxicity of compound **1** was evaluated using the previously described method [32] using MTT cell proliferation assay kits. The following three cancer cell lines have been studied: Breast cancer cell lines (MCF-7), colon cancer cell lines (HT-29), and hepatocellular carcinoma cell lines (HepG2). The cells were cultured in RPMI-1640 at 37°C with 5% CO_2, supplemented with 10% FBS, penicillin, and streptomycin sulfate. They were grown in a 96-well flat-bottom plate (200 µL, 1×10^5 cells/well, in triplicate) and incubated for 24 h. After that, DMSO solutions of the residues at concentrations of 30 and 100 µg/mL were added to the wells. Then, the treated cells were incubated for 48 h at 37°C, followed by the MTT assay. The absorbance (OD; λ = 570 nm) was recorded, and the cell survival was determined using non-linear regression analysis. Camptothecin (Sigma-Aldrich, St. Louis, Missouri, USA) was used as a positive control.

CONCLUSION

A unique coumarin featuring a rare 2-hydroxypropanoic acid side chain, named artabscoumarin (**1**), and four phenolic and flavonoid compounds were isolated and characterized from the aerial parts of *A. absinthium*. The structure of the isolated compounds was determined by extensive spectroscopic analysis as well as mass spectrometric data. Artabscoumarin (**1**) exhibited moderate cytotoxic activity against cancer cell lines.

SUPPORTING INFORMATION

The supplementary material is available with the authors for future correspondence.

ACKNOWLEDGMENTS

The authors gratefully acknowledge the funding of the Deanship of Graduate Studies and Scientific Research, Jazan University, Saudi Arabia, through project number: (RG24-S072).

REFERENCES

[1] Erel, S.B., Reznicek, G., Şenol, S.G., Yavaşoğlu, N.Ü.K., Konyalioğlu, S. and Zeybek, A.U. Antimicrobial and antioxidant properties of *Artemisia* L. species from Western Anatolia, *Turk. J. Biol*., **2012**, *36*, 75–84.

[2] Mohammed, H.A. Phytochemical analysis, antioxidant potential, and cytotoxicity evaluation of traditionally used *Artemisia absinthium* L. (Wormwood) growing in the central region of Saudi Arabia, *Plants* (*Basel*), **2022**, *11*, 1028–1041.

[3] Bora, K.S. and Sharma, A. Phytochemical and pharmacological potential of *Artemisia absinthium* Linn. and *Artemisia asiatica* Nakai: A review, *J. Pharm. Res*., **2010**, *3*, 325–328.

[4] Canadanovic-Brunet, J.M., Djilas, S.M., Cetkovic, G.S. and Tumbas, V.T. Free-radical scavenging activity of wormwood (*Artemisia absinthium* L.) extracts, *J. Sci. Food Agric.*, **2005**, *85*, 265–272.

[5] Da Silva, J.A.T. Mining the essential oils of the *Anthemideae*, *Afr. J. Biotechnol*., **2004**, *3*, 706–720.

[6] Msaada, K., Salem, N., Bachrouch, O., Bousselmi, S., Tammar, S., Alfaify, A., Al Sane, K., Ben Ammar, W., Azeiz, S., Haj Brahim, A., Hammami, M., Selmi, S., Limam, F. and Marzouk, B. Chemical composition and antioxidant and antimicrobial activities of Wormwood (*Artemisia absinthium* L.) essential oils and phenolics, *J. Chem*., **2015**, *2015*, 804658.

[7] Kordali, S., Cakir, A., Mavi, A., Kilic, H. and Yildirim, A. Screening of chemical composition and antifungal and antioxidant activities of the essential oils from three Turkish *Artemisia* species, *J. Agric. Food Chem*., **2005**, *53*, 1408–1416.

[8] Irshad, S., Butt, M. and Younus, H. *In-vitro* antibacterial activity of two medicinal plants neem (*Azadirachta indica*) and peppermint, *Int. Res. J. Pharm*., **2011**, *1*, 9–14.

[9] Zafar, M., Hamdard, M. and Hameed, A. Screening of *Artemisia absinthium* for antimalarial effects on *Plasmodium berghei* in mice: A preliminary report, *J. Ethnopharmacol*., **1990**, *30*, 223–326.

[10] Khattak, S.G., Gilani, S.N. and Ikram, M. Antipyretic studies on some indigenous Pakistani medicinal plants, *J. Ethnopharmacol*., **1985**, *14*, 45–51.

[11] Nibret, E. and Wink, M. Volatile components of four Ethiopian *Artemisia* species extracts and their *in vitro* antitrypanosomal and cytotoxic activities,

Phytomedicine, **2010**, *17*, 369–374.

[12] Chopra, C., Bhatia, M. and Chopra, I. *In vitro* antibacterial activity of oils from Indian medicinal plants, *J. Am. Pharm. Assoc*., **1960**, *49*, 780–781.

[13] Chiasson, H., Bélanger, A., Bostanian, N., Vincent, C. and Poliquin, A. Acaricidal properties of *Artemisia absinthium* and *Tanacetum vulgare* (Asteraceae) essential oils obtained by three methods of extraction, *J. Econ. Entomol*., **2001**, *94*, 167–171.

[14] Mahmoudi, M., Ebrahimzadeh, M.A., Ansaroudi, F., Nabavi, S.F. and Nabavi, S.M Antidepressant and antioxidant activities of *Artemisia absinthium* L. at flowering stage, *Afr. J. Biotechnol*., **2009**, *8*, 7170–7175.

[15] Ahmad, F., Khan, R.A. and Rasheed, S. Study of analgesic and anti-inflammatory activity from plant extracts of *Lactuca scariola* and *Artemisia absinthium*, *J. Islamic World Acad. Sci.*, **1992**, *5*, 111–114.

[16] Wang, Y., Hamburger, M., Gueho, J. and Hostettemann, K. Antimicrobial flavonoids from *Psiadia trinervia* and their methylated and acetylated derivatives, *Phytochemistry*, **1989**, *28*, 2323–2327.

[17] Menkham, S. and Suttisri, R. Chemical constituents of *Cleidion spiciflorum* leaves, *Thai. J. Pharm. Sci*., **2003**, *27*, 33–39.

[18] Han, X., Ma, X., Zhang, T., Zhang, Y., Liu, Q. and Ito, Y. Isolation of high-purity casticin from *Artemisia annua* L. by high-speed counter-current chromatography, *J. Chromatogr. A*, **2007**, *1151*, 180–182.

[19] Hajdú, Z., Hohmann, J., Forgo, P., Martinek, T., Dervarics, M., Zupkó, I., Falkay, G., Cossuta, D. and Máthé, I. Diterpenoids and flavonoids from the fruits of *Vitex agnus-castus* and antioxidant activity of the fruit extracts and their constituents, *Phytother. Res*., **2007**, *21*, 391–394.

[20] Gao, H., Wang, H., Li, G., Du, X., Zhang, X., Han, Y., Huang, J., Li, X. and Wang, J. Constituents from Zhuyeqing Liquor and their inhibitory effects on nitric oxide production, *Phytochem. Lett*., **2014**, *7*, 150–155.

[21] Martínez, V., Barberá, O., Parareda, J.S. and Marco, J.A. Phenolic and acetylenic metabolites from *Artemisia assoana*, *Phytochemistry*, **1987**, *26*, 2619–2624.

[22] Xie, Y.Y., Yuan, D., Yang, Y., Wang, L.H. and Wu, C.F. Cytotoxic activity of flavonoids from the flowers of *Chrysanthemum morifoliumon* human colon cancer Colon205 cells, *J. Asian. Nat. Prod. Res*., **2009**, *11*, 771–778.

[23] Murray, R.D.H., Mendez, J. and Brown, S.A. *The Natural Coumarins: Occurrence, Chemistry and Biochemistry*. Chichester, John Wiley, **1982**.

[24] Girard, C., Roux, D., Muyard, F., Colombain, M., Tillequin, F., Waterman, P.G. and Bevalot, F. 3-Substituted coumarins from the Twigs of *Rhadinothamnus rudis* ssp. *Amblycarpus*, *Z. Naturforsch. B*, **2005**, *60b*, 561–564.

[25] Szabo, G., Greger, H. and Hofer, O. Coumarin-hemiterpene ethers from *Artemisia* species, *Phytochemistry*, **1985**, *24*, 537–554.

[26] Meng, L., Yu, C., Hui, J., Jiang, N., Wang, H., Xie, J., Xu, L. and Liu, Y. Three new coumarin derivatives from *Maytenus hookeri*, *Nat. Prod. Res*., **2022**, *38*, 365–371.

[27] Lei, L., Xue, Y.B., Liu, Z., Peng, S.S., He, Y., Zhang, Y., Fang, R., Wang, J.P., Luo, Z.W., Yao, G.M., Zhang, J.W., Zhang, G., Song, H.P. and Zhang, Y.H. Coumarin derivatives from *Ainsliaea fragrans* and their anticoagulant activity, *Sci. Rep*., **2005**, *5*, 13544.

[28] Maneerat, W., Prawat, U., Saewan, N. and Laphookhieo, S. New coumarins from *Clausena lansium* twigs, *J. Braz. Chem. Soc*., **2010**, *21*, 665–668.

[29] Cao, N.K., Chen, Y.M., Zhu, S.S., Zeng, K.W., Zhao, M.B., Li, J., Tu, P.E. and Jiang, Y. Three new coumarins and a new coumarin glycoside from *Micromelum integerrimum*. *Chin. J. Nat. Med.*, **2012**, *19*, 621–625.

[30] Wang, Y.S., He, H.P., Yang, J.H., Di, Y.T. and Hao, K.J. New monoterpenoid coumarins from *Clausena anisum-olens*, *Molecules*, **2008**, *13*, 931–937.

[31] Aminudin, N.I., Ahmad, F., Taher, M. and Zulkifli, R.M. Incrassamarin A-D: Four new 4-substituted coumarins from *Calophyllum incrassatum* and their biological activities, *Phytochem. Lett*., **2016**, *16*, 287–293.

[32] Mosmann, T. Rapid colorimetric assay for cellular growth and survival: Application to proliferation and cytotoxicity assays, *J. Immunol. Methods*, **1983**, *65*, 55–63.

Received: 11 Jan 2025; Accepted: 04 Feb 2025